Geochimica et Cosmochimica Acta 350 (2023) 87–105

Contents lists available at ScienceDirect

Geochimica et Cosmochimica Acta

journal homepage: www.elsevier.com/locate/gca

# Plume–lithosphere interactions and LIP-triggered climate crises constrained by the origin of Karoo lamproites

Sebastian Tappe [a,b,*], Ntando S. Ngwenya [b], Andreas Stracke [c], Rolf L. Romer [d], Johannes Glodny [d], Axel K. Schmitt [e,f]

[a] Department of Geosciences, UiT – The Arctic University of Norway, 9037 Tromsø, Norway
[b] Department of Geology, University of Johannesburg, 2006 Auckland Park, South Africa
[c] Institut für Mineralogie, Westfälische Wilhelms-Universität, Corrensstrasse 24, 48149 Münster, Germany
[d] Helmholtz-Zentrum Potsdam Deutsches GeoForschungsZentrum GFZ, Telegrafenberg, 14473 Potsdam, Germany
[e] Institut für Geowissenschaften, Universität Heidelberg, Im Neuenheimer Feld 236, 69120 Heidelberg, Germany
[f] John de Laeter Centre, Curtin University, 6845 Bentley, Australia

ARTICLE INFO

*Associate editor:* Tomas Magna

*Keywords:*
Failed cratonic rift
SIMS U–Pb perovskite geochronology
Sr–Nd–Hf–Pb–Li isotopes
Trace elements in olivine
East African Rift
Volcanic $SO_2$ emission
Large igneous provinces

ABSTRACT

We identified a ca. 180 Ma diamondiferous lamproite event in Zambia, establishing a link between ultrapotassic volcanism and the early Jurassic Karoo flood basalt province of sub-Saharan Africa. The cratonic lamproites erupted through the Permo–Triassic Luangwa Rift structure, but MgO-rich ultrapotassic magma formation was unrelated to rifting and triggered by plume–lithosphere interactions during the Karoo LIP event. Elevated Li–Zn–Ti concentrations in magmatic olivine (up to 18.5 ppm Li at 86–90 mol.% forsterite) and strong Sr–Nd–Hf–Pb isotopic enrichment of the host lamproites ($^{87}Sr/^{86}Sr$ = 0.70701–0.70855, εNd = −10.8 to −10, εHf = −20.3 to −19.1, $^{206}Pb/^{204}Pb$ = 16.8–17.5) suggest partial melting of phlogopite-metasomatized lithospheric mantle domains, at approximately 180–200 km depth. The mantle-like $\delta^7Li$ values (+2.8 to +5.7‰) of the most pristine lamproite samples are compatible with source enrichment by asthenosphere-derived melts, without significant involvement of recycled sedimentary components. This geochemical fingerprint stands in sharp contrast to the negative $\delta^7Li$ compositions of primitive K-rich volcanic rocks from collision zone settings, where the shallow mantle sources contain recycled sediment.

Isotope modelling demonstrates that the sub-Saharan lamproites originate from a MARID-style metasomatized peridotitic mantle source that underwent incompatible element enrichment at ca. 1 Ga, during tectonic activity associated with Rodinia supercontinent formation. Plume-sourced basaltic and picritic magmas of the 180 Ma Karoo LIP interacted with such K-rich hydrous lithospheric mantle domains, thereby attaining enriched incompatible element and radiogenic isotope compositions. Nd–Hf isotope mass balance suggests that up to 25% of MARID-sourced lamproite melt component contributed to some of the high-Ti flood volcanic units.

Although large quantities of volatiles can be transferred from Earth's mantle to the atmosphere via plume–lithosphere interactions, it is unlikely that outgassing of mantle-sourced sulphur can exceed the climatic impact caused by the release of much more abundant carbon from thick continental roots. Thus, the excess $SO_2$ required to account for transient atmospheric cooling during the early Jurassic, coincident with the Karoo LIP event, must have had a thermogenic origin near the surface of Earth.

## 1. Introduction

Anomalously large, episodic mantle melting events away from tectonic plate boundaries provide glimpses of the dynamic deep Earth. Such melting events are manifested in Large Igneous Provinces (LIPs), which were emplaced at crustal levels during short-pulsed mafic-dominated magma eruptions since the Archean (Coffin and Eldholm, 1992; Ernst, 2014). Key to understanding LIP-sized melting anomalies is the geologic record of well-preserved Mesozoic–Cenozoic continental flood basalt occurrences that may herald supercontinent breakup and develop into volcanic rifted margins (White and McKenzie, 1989). The ca. 180 Ma Karoo LIP in southern Africa and East Antarctica presents a classic

* Corresponding author at: Department of Geosciences, UiT The Arctic University of Norway, P.O. Box 6050 Langnes, N-9037 Tromsø, Norway.
*E-mail address:* sebastian.tappe@uit.no (S. Tappe).

https://doi.org/10.1016/j.gca.2023.04.008
Received 22 October 2022; Accepted 13 April 2023
Available online 20 April 2023

continental flood basalt province that has been linked to the initial stage of Gondwana breakup (Cox, 1992). More than 2 $Mkm^3$ of basaltic magmas were emplaced as lavas, sills and dykes between 183 and 177 Ma (Greber et al., 2020), but subordinate volumes of early-stage picritic and nephelinitic–carbonatitic magmas as well as late-stage rhyolitic lavas also occur (Harmer et al., 1998; Turunen et al., 2019).

Although temporal links between flood volcanism and climate change have been established by high-precision geochronology (Hofmann et al., 1997; Kasbohm and Schoene, 2018; Greber et al., 2020), the causal links, if any, are contentious. For example, rapidly emitted volatiles (e.g., $CO_2$, $SO_2$, HCl) responsible for atmospheric temperature fluctuations (Black et al., 2021) are argued by some workers to be sourced mainly from the mantle-derived magmas (Sobolev et al., 2011; Guex et al., 2016; Capriolo et al., 2020), whereas others put emphasis on a thermogenic origin of these volatile components, invoking sedimentary country rocks as the source (Svensen et al., 2007; Ganino and Arndt, 2009; Heimdal et al., 2020). Importantly, it has been suggested that intensive biotic mass extinctions are associated mainly with LIPs on continental shields underpinned by thick mantle roots, such as the ca. 250 Ma Siberian Traps and ca. 65 Ma Deccan LIP (Guex et al., 2016). Using the ca. 180 Ma Karoo LIP as an example, these authors argued that critical amounts of $SO_2$ had been released into the atmosphere via early-stage alkaline magmatism sourced from volatile-enriched (e.g., sulphide-bearing) cratonic mantle lithosphere that was reactivated during plume impingement.

The majority of petrogenetic models for continental flood basalt volcanism invoke mantle plume sources (Ernst, 2014), with plume–lithosphere interactions, fractional crystallization and crustal contamination playing variable roles in magma type diversification, such as the common low-Ti and high-Ti groupings of volcanic suites (Cox, 1992; Arndt et al., 1993; Gibson et al., 1996; Jourdan et al., 2007; Heinonen et al., 2016). For the Karoo LIP in particular, several studies identified strong incompatible element and isotopic enrichment of certain picritic to basaltic volcanic suites in southern Africa and East Antarctica (Ellam et al., 1992; Gallagher and Hawkesworth, 1992; Riley et al., 2005; Jourdan et al., 2007; Harris et al., 2015; Luttinen, 2018). Some of these enriched signatures may be caused by melt contributions from metasomatized cratonic mantle lithosphere to more depleted plume-sourced magmas (Ellam and Cox, 1991; Riley et al., 2005; Jourdan et al., 2007; Heinonen et al., 2010). However, such models rely on assumptions about the nature of the reactivated metasomatic components.

We identified a ca. 180 Ma old diamondiferous lamproite magmatic event beneath the cratonic Luangwa Rift of eastern Zambia, positioned in the northern Karoo LIP. The MgO-rich ultrapotassic lavas constrain the nature of relatively 'pure' alkali-metasomatic mantle components including volatile budgets, potentially available for flood basalt volcanism. Olivine trace element and bulk-rock Sr–Nd–Hf–Pb–Li isotope data for the lamproites, in concert with geochemical modelling, provide new insights into the deep origins of K-rich hydrous magmas, including their geodynamic and environmental significance for plume–lithosphere interactions.

## 2. Background

### 2.1. The ca. 300–200 Ma Karoo rift basins of interior Gondwana

Diamondiferous lamproites are known from the ca. 300–200 Ma Luangwa Rift of eastern Zambia since the 1970s (Scott Smith et al., 1989), but these so-called Kapamba lamproites have only recently been associated with the ca. 180 Ma Karoo LIP in sub-Saharan Africa (Ngwenya and Tappe, 2021; this study) (Fig. 1). The ~600 km long and on average ~60 km wide Luangwa Valley is part of a larger Permo–Triassic Karoo rift basin system stretching from Tanzania in the NE to Zimbabwe in the SW (Fig. 2). The Luangwa Rift formed within the Irumide Belt (Daly et al., 1989), which presents variably reworked and rejuvenated 'metacratonic' lithosphere between the Congo–Tanzania–(*Bangweulu*) craton to the north and the Kalahari craton to the south (De Waele et al., 2006). These large, composite Archean cratons assembled during the Pan-African orogeny at 550–520 Ma (Goscombe et al., 2020), but the intervening mobile belts record collision events throughout the Proterozoic, with the 1050–950 Ma Irumide orogeny being most prominent (De Waele et al., 2006). Despite protracted crustal deformation, the lithosphere beneath the Irumide Belt is >180 km thick (Sarafian et al., 2018; Ngwenya and Tappe, 2021), which is marginally thinner than the 200–230 km thick lithospheres of neighbouring cratons (Celli et al., 2020).

Steep Proterozoic shear zones along the Irumide Belt facilitated development of extensive pull-apart basins during Permo–Triassic intraplate tectonics, including the half-graben structures that form the Luangwa Rift (Burke and Dewey, 1973; Daly et al., 1989; Banks et al., 1995) (Fig. 2). These strike-slip movements of Proterozoic basement between Archean blocks created the narrow fault-bounded accommodation space for some of the thickest sedimentary successions (up to 8 km) known from the ca. 300–200 Ma Karoo Supergroup (Catuneanu et al., 2005). The 'failed' cratonic Luangwa Rift is experiencing neotectonic activity associated with the adjoining East African Rift System (Fig. 2), as is recently witnessed by minor extension and elevated seismicity (Wedmore et al., 2021).

### 2.2. Geographic extent of the ca. 180 Ma Karoo LIP

Remnants of the 183–177 Ma Karoo LIP occur in sub-Saharan Africa and East Antarctica, and the estimated magma volumes of >2 $Mkm^3$ place this event among the most-voluminous continental LIPs globally (Cox, 1992; Ernst, 2014). The scattered nature of volcanic outcrops across a 6 $Mkm^2$ region in central and southern Africa suggests that the Karoo LIP has been eroded significantly. The main eruptive centres were located at triple junctions around the Zimbabwe craton (Nuanetsi and Zambesi 'plume' centres), based on the convergence of mafic dyke swarms and Karoo rift basins (Burke and Dewey, 1973).

Uncertainty surrounds the northern extent of the Karoo LIP, which may reach onto the Tanzania craton all the way to the equator, based on aeromagnetic evidence (Halls et al., 1987). Indeed, new U–Pb baddeleyite data reveal an age of 181 ± 7 Ma for a north-trending 30-m-thick dolerite dyke in western Tanzania (Ernst et al., 2015), forming part of the inferred Karoo-age swarm that can be traced from eastern Zambia into Tanzania (Halls et al., 1987). Furthermore, several carbonatite bodies along the rifted SW margin of the Tanzania craton are inferred to be of Karoo LIP age (Harmer and Nex, 2016). These observations suggest that the Karoo LIP has a sizeable northern lobe that may push the province outline northward by >500 km (Ernst et al., 2015), and they demonstrate that the lamproites in eastern Zambia fall firmly within the boundaries of the northern Karoo LIP (Fig. 1b).

### 2.3. Diamondiferous lamproites of the cratonic Luangwa Rift

Mode of occurrence of the Kapamba lamproites (14 pipe-like bodies and several dykes) and their petrography have been described by Scott Smith et al. (1989). We revisited the 20 × 25 km large volcanic field in the South Luangwa National Park in 2018 to undertake detailed sampling of Kapamba Pipe-6 and Pipe-10a (an archival sample was obtained for Pipe-1). Comprehensive petrography, EPMA-determined mineralogy and major element geochemistry of the lamproites are reported in Ngwenya and Tappe (2021). This study concluded that relatively primitive olivine–leucite lamproite magmas of 'anorogenic' affinity fed the low-volume phreatomagmatic eruptions at Kapamba, with some compositional resemblance to kamafugites from the western branch of the East African Rift System and to orangeites from the Kaapvaal craton in southern Africa. Analysis of peridotite-derived, forsterite-rich olivine xenocrysts suggests that the cratonic Luangwa Rift retained a relatively cold (≤42 $mW/m^2$) lithospheric root down to ~180–200 km depth

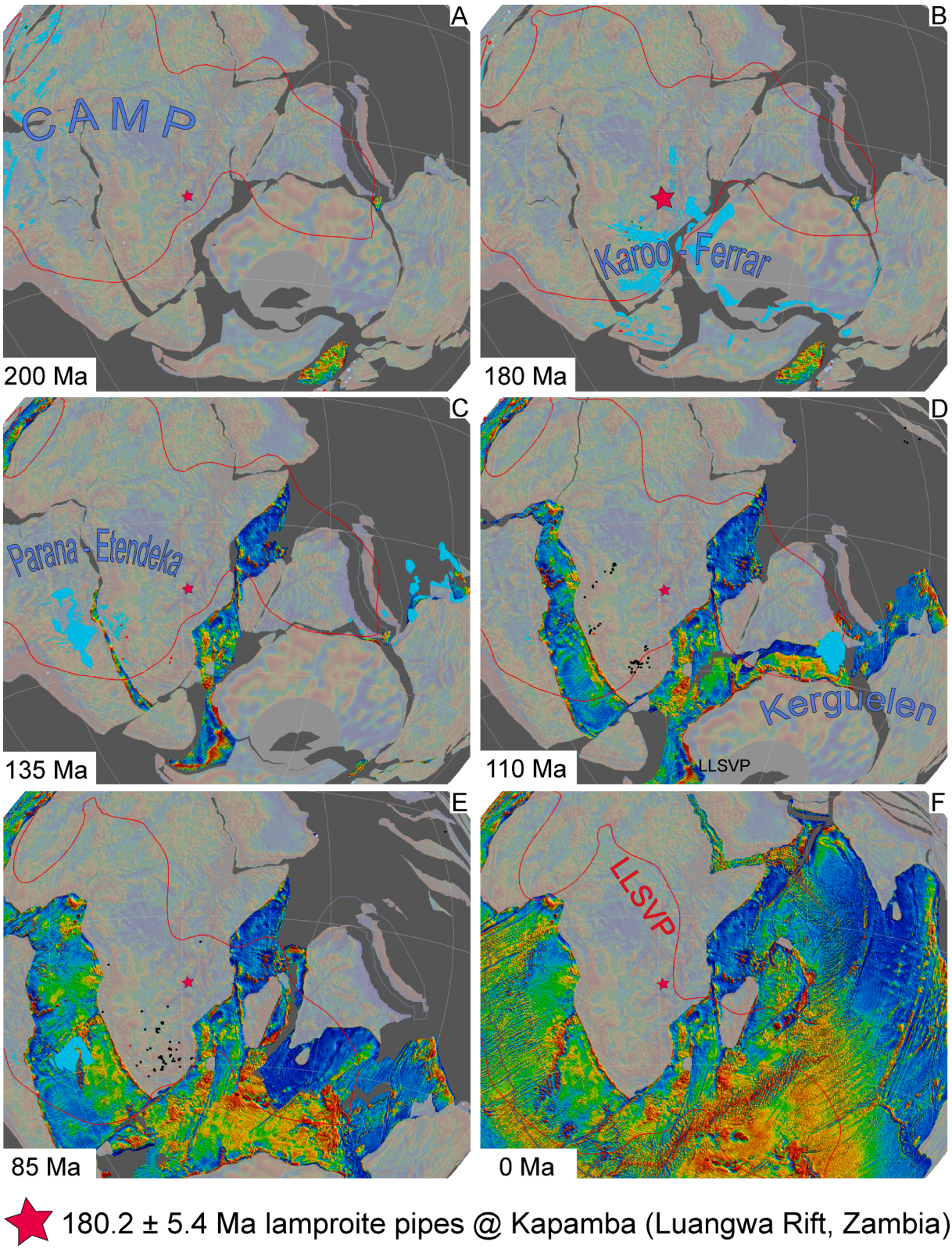


**Fig. 1.** Plate-tectonic reconstructions of Gondwanan elements between 200 Ma and present-day using the GPlates software (Müller et al., 2018), with magnetic signatures for continental and oceanic lithospheres as backdrop **(A-F)**. Volcanic products of Mesozoic LIPs are shown in light blue at 200 Ma (Central Atlantic Magmatic Province), 180 Ma (Karoo–Ferrar LIP), 135 Ma (Parana–Etendeka LIP) and 110 Ma (Kerguelen LIP). The red star in all panels indicates the location of the ca. 180 Ma old Kapamba lamproites **(A–F)**, and in **Panel B** the spatiotemporal association with the Karoo LIP is evident. Major episodes of kimberlite magma eruptions across sub-Saharan Africa are shown as small black circles at 110 Ma **(D)** and 85 Ma **(E)**. The thin red outline in all panels **(A–F)** corresponds to the 0.9% slow-contour in the *s10mean* seismic tomography model for the African LLSVP at 2800 km depth. Kimberlite data and the original parameter sources for the LLSVP model are provided in Tappe et al. (2018).

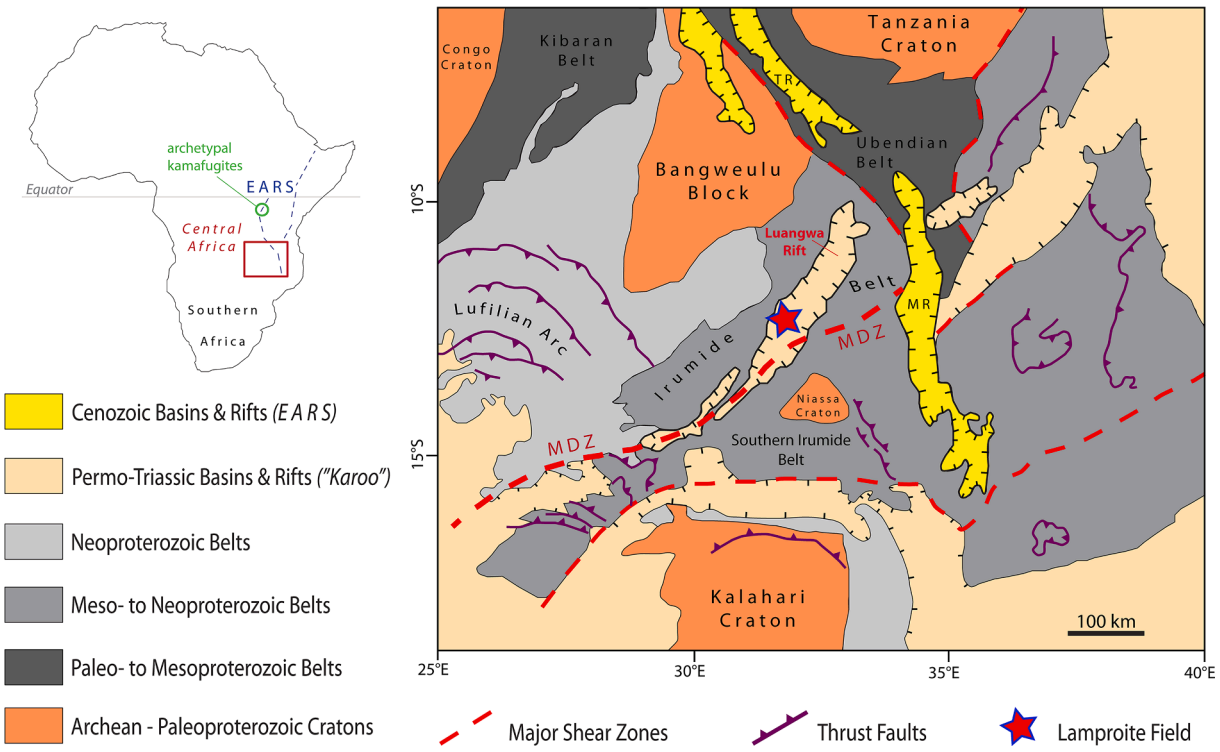


**Fig. 2.** Geological map of south-central Africa (Sarafian et al., 2018), where the red star locates the ca. 180 Ma Kapamba lamproites within the 'failed' Permo–Triassic Luangwa Rift structure (Ngwenya and Tappe, 2021). The intracontinental rift developed within the Proterozoic Irumide Belt between the composite Congo–Tanzania–*Bangweulu* craton to the north and the Kalahari craton to the south. A major strike-slip reactivation event along the ca. 1 Ga old Mwembeshi Dislocation Zone (MDZ) created pull-apart basins during Permo–Triassic times forming part of the Luangwa Valley rift system in eastern Zambia. The prominent north–south oriented Cenozoic rift basins represent the southern extension of the currently active East African Rift System (EARS). MR – Malawi Rift, TR – Tanganyika Rift.

during Mesozoic lamproite volcanism, in agreement with the mostly amagmatic nature of this failed branch. Ngwenya and Tappe (2021) argued that the Kapamba lamproites and type kamafugites represent melting products of similar K-metasomatized cratonic mantle domains, but that magma formation occurred under contrasting volatile conditions (i.e., $H_2O$–F-rich *vs* $CO_2$–$H_2O$–F-rich) at different stages during rift development (i.e., incipient *vs* slightly more advanced rifting). Although similar K-metasomatized cratonic mantle sources are required in the formation of Kaapvaal orangeites, melting may occur at even greater depths and without the direct influence of rifting (Giuliani et al., 2015). In the study presented here, we revise the previously suggested link between development of the Luangwa Rift and lamproite magma eruptions at Kapamba using new evidence from geochronology and radiogenic isotope systematics (Section 4.2.1).

## 3. Results

We report the first U–Pb age determination for lamproite magma emplacement in the Luangwa Rift, as well as trace element and Sr–Nd–Hf–Pb–Li isotopic compositions for our 2018 sample collection. Analytical methods are described in Supplementary file A, and all data including those for reference materials are reported in Supplementary file B. This repository also hosts the bulk lamproite major element and olivine xenocryst data (major and trace elements) originally reported in Ngwenya and Tappe (2021), plus new geochemical analyses for a variety of country rocks from Luangwa Valley.

### 3.1. U–Pb perovskite age of lamproite magmatism in the Luangwa Rift structure

The Kapamba lamproite magmas erupted through a >4 km thick clastic-dominated sedimentary succession of the Karoo Supergroup, where the uppermost members of the Middle Triassic Ntawere Formation contain the tetrapod fossils *Sangusaurus* and *Zambiasaurus* of the Anisian to Ladinian stages (Angielczyk et al., 2014). This biostratigraphic information constrains magma emplacement to <230–240 Ma, in agreement with the previous estimate of 220 Ma (Scott Smith et al., 1989). These authors noted, however, that previous $^{87}Rb$–$^{87}Sr$ and $^{40}Ar/^{39}Ar$ analyses on phlogopite have poor precision, with age results scattering between 255 and 160 Ma. Unfortunately, lack of documentation prevents an assessment of the possible geological meaning of the dates quoted above.

We collected U–Pb perovskite data by secondary ionization mass spectrometry (SIMS) to better constrain the timing of lamproite magma emplacement (Supplementary Material for methods). The accuracy of young U–Pb perovskite ages (i.e., Mesozoic–Cenozoic) relies heavily on accurate corrections for the presence of initial common-Pb, which typically accounts for >30% of the $^{206}Pb$ inventory in crystals with <100 ppm U (Kinny et al., 1997). The six perovskite crystals analysed from four individual lamproite samples of Pipe-10a (Fig. 3) have relatively low U contents between 40 and 100 ppm, and the total $^{206}Pb$ comprises 72–79% common-$^{206}Pb$ (Supplementary Material).

The presence of initial common-Pb was corrected using the average $^{206}Pb/^{204}Pb$ of 16.91 ± 0.04 (n = 9) and $^{207}Pb/^{206}Pb$ of 0.9185 ± 0.002 (n = 9) for nine individual lamproite lava samples from Pipe-10a. These Pb isotopic compositions were independently determined by solution-mode MC-ICP-MS analysis (Supplementary Material). The lamproite material from Pipe-10a yielded a weighted average $^{206}Pb/^{238}U$ perovskite age of 180.2 ± 5.4 Ma (2S.E.; MSWD = 0.95; Fig. 4). To evaluate the robustness of the $^{207}Pb$-corrected $^{206}Pb/^{238}U$ perovskite age, the uncorrected U–Pb data were regressed in Tera–Wasserburg space anchoring the composition of common-$^{207}Pb/^{206}Pb$ at 0.9185 (see

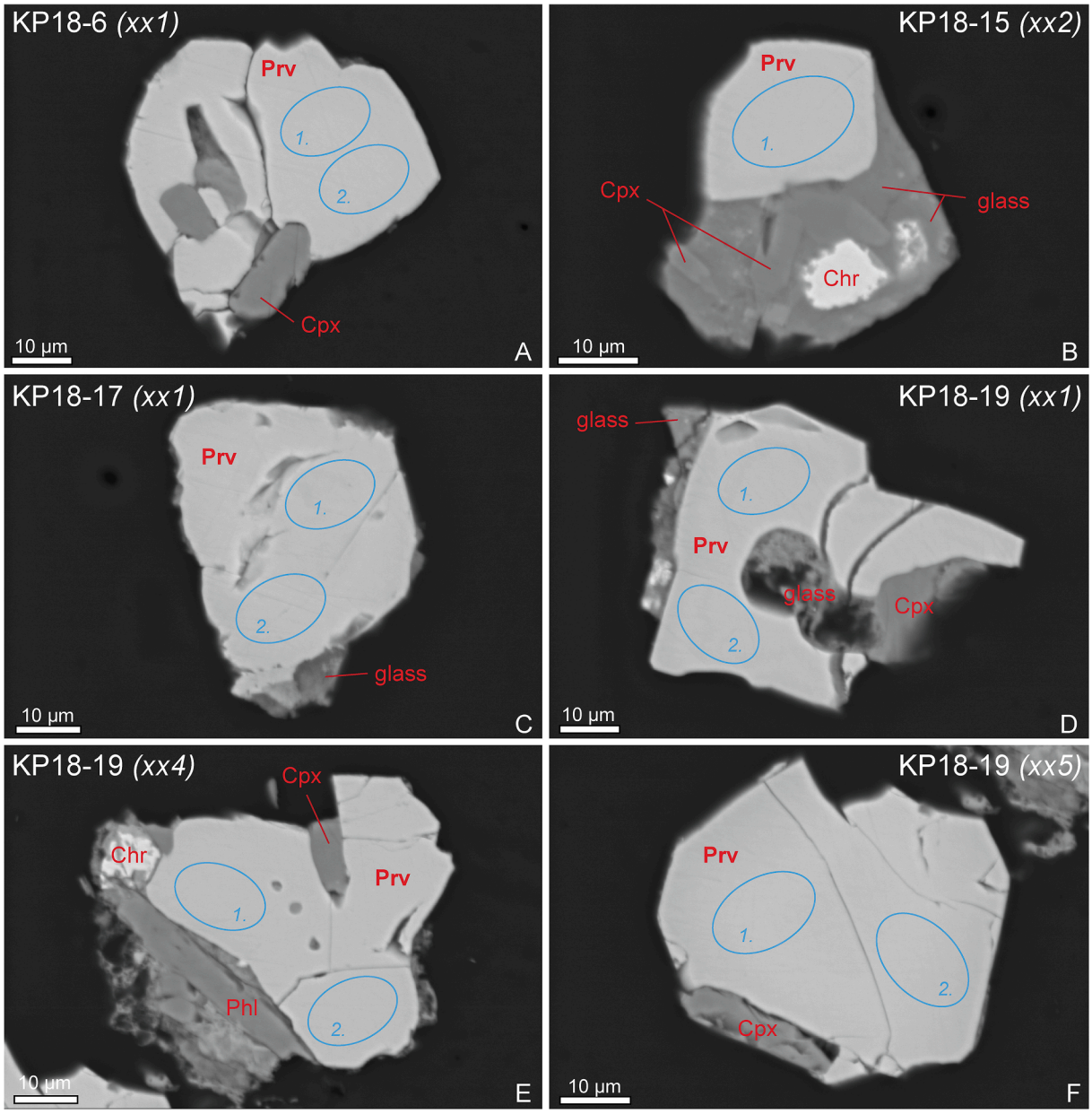


**Fig. 3.** Backscattered electron images **(A-F)** of 'micro-rock' fragments <50 µm in diameter from Kapamba lamproite Pipe-10a, containing fresh unzoned and inclusion-free perovskite crystals. The perovskite crystals displayed in **Panels A** to **F** were analysed by SIMS for their U–Th–Pb isotopic compositions, and the 11 spot analyses (10 × 15 µm wide blue ellipses) are pooled into a $^{207}$Pb-corrected weighted average $^{206}$Pb/$^{238}$U age of 180.2 ± 5.4 Ma (Fig. 4b). Sample identifiers refer to the U–Pb isotope data listed in the Supplementary Material. Chr – chromite, Cpx – clinopyroxene, Phl – phlogopite, Prv – perovskite.

above). This treatment of our U–Pb data yielded a concordia intercept age of 178.1 ± 8.4 Ma (2S.E.; MSWD = 0.54; Fig. 4). Importantly, both $^{207}$Pb-corrected ages are in good agreement with the $^{204}$Pb-corrected $^{206}$Pb/$^{238}$U age of 176 ± 16 Ma (2S.E.; MSWD = 0.46; not shown), providing firm control on the accuracy of the early Jurassic U–Pb perovskite age. In alignment with numerous *in-situ* U–Pb perovskite studies on Mesozoic–Cenozoic kimberlites and related rocks (Smith et al., 1994; Batumike et al., 2008; Griffin et al., 2014; Sun et al., 2014), the Tera–Wasserburg concordia intercept age is preferred here, and we consider 178.1 ± 8.4 Ma as the current best age estimate of lamproite magma emplacement in Luangwa Valley.

### 3.2. Minor and trace elements in lamproite-hosted magmatic olivine

Fresh olivine microphenocrysts occur together with rare mantle-derived olivine xenocrysts in lamproite lavas from Kapamba Pipe-6 and Pipe-10a (Fig. 5a). The microphenocryst cores have forsterite contents between 86 and 90 mol.%, lower than the forsterite contents of the peridotite-derived xenocrysts (90–93 mol.%; Ngwenya and Tappe, 2021). The olivine microphenocrysts exhibit overgrowths and rims with forsterite contents between 80 and 86 mol.% (Fig. 5a). The primitive microphenocryst cores have relatively low Ni/Mg and Mn/Fe ratios (Fig. 5b). They have notably higher Ca (820–2300 ppm) and Ti (54–138 ppm) concentrations than the mantle-derived olivine xenocrysts (<400 ppm Ca and <30 ppm Ti; Ngwenya and Tappe, 2021). Their Ca–Ti systematics resemble those of olivine phenocrysts in Karoo LIP picrite lavas and sills (Howarth and Harris, 2017) (Fig. 5c). However, lamproitic olivine from the Luangwa Rift has much higher Li (4.2–18.5 ppm) but significantly lower Zn (102–143 ppm) concentrations than picritic olivine from the Karoo LIP (Fig. 6). Further trace elements with significance for distinguishing between magmatic and xenocrystic olivine are: Cr (283–652 *vs* 16–356 ppm), Na (118–327 *vs* 15–142 ppm), Al (70–164

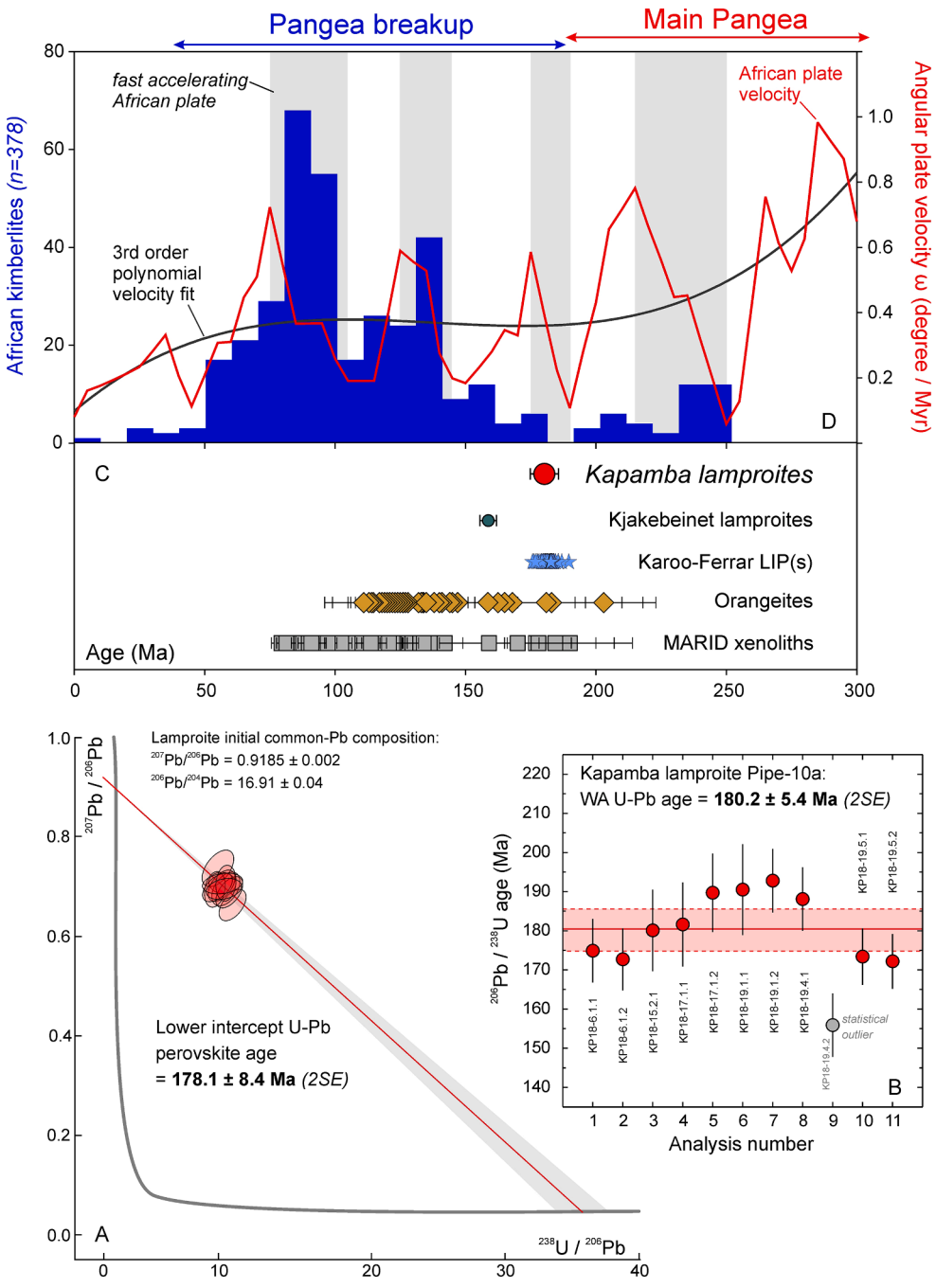


**Fig. 4.** The first U–Pb age determination (SIMS) for the diamondiferous lamproite magmatic event in the Luangwa Rift structure of sub-Saharan Africa, with comparisons to the timing of other mantle-derived magmatic events that accompanied Mesozoic Pangea–Gondwana breakup across southern Africa and East Antarctica **(A-D). (A)** Tera–Wasserburg U–Pb concordia diagram for perovskite crystals from Kapamba lamproite Pipe-10a (Fig. 3). The intercept age of 178.1 ± 8.4 Ma was obtained by anchoring the data regression line at an initial common-Pb isotopic composition independently determined on host lamproite material by solution-mode MC–ICP–MS analysis (Supplementary Material). This $^{207}$Pb-corrected age is identical within its 2S.E. uncertainty to the $^{207}$Pb-corrected weighted average $^{206}$Pb/$^{238}$U age of 180.2 ± 5.4 Ma **(B). (C)** Comparison of the SIMS-determined U–Pb age for the Kapamba lamproites with the ages of pertinent Mesozoic magmatic events in Gondwanaland, such as the Kjakebeinet lamproites in East Antarctica (Luttinen et al., 2002), the Karoo–Ferrar LIP in sub-Saharan Africa and East Antarctica (Greber et al., 2020), the Group-2 kimberlite or orangeite pulses in South Africa (Tappe et al., 2018), and the formation of strongly K-metasomatized lithospheric mantle (MARID xenoliths) within the Kaapvaal craton root of southern Africa (Hoare et al., 2021). **(D)** Frequency distribution of emplacement ages for African Group-1 kimberlites overlain by the African tectonic plate velocity since Pangea–Gondwana stabilization at ca. 300 Ma (Tappe et al., 2018). The Kapamba lamproite magmatic event at ca. 180 Ma marks the onset of the main episode of Mesozoic–Cenozoic kimberlite and related volcanism across Africa, which was intimately associated with the breakup of Gondwanaland.

*vs* 15–77 ppm), P (100–1330 *vs* <56 ppm) and Sc (2.6–3.7 *vs* 4.8–7.8 ppm) (Supplementary Material).

### 3.3. Geochemistry of the Kapamba lamproites

#### 3.3.1. Major and trace element compositions

Mineralogy and bulk major element compositions identify the $CO_2$-free (i.e., devoid of modal carbonates) volcanic rocks at Kapamba as olivine–leucite lamproites, with MgO contents of >10 wt%, but relatively low $K_2O$ down to 1.6 wt%. Ngwenya and Tappe (2021) discovered that the low $K_2O$ contents are linked to the highly efficient conversion of leucite to analcime in the otherwise very fresh volcanic rocks. They calculated primary $K_2O$ contents of up to 9 wt% (original $K_2O/Na_2O$ ratios of up to 6), suggesting that the volcanic activity within the Luangwa Rift structure was truly ultrapotassic in nature.

The Kapamba lamproites are enriched in highly incompatible elements, with mantle-normalized distributions similar to those of Kaapvaal orangeites (Fig. 7a). Common features of the Kapamba lamproites and Kaapvaal orangeites are their strong Cs–Ba enrichments coupled to relative depletions of certain HFSE such as Th–U (note that only a few orangeite occurrences are characterized by Th–U enrichment). However, the incompatible element patterns (from Th to Lu) of the Kapamba lamproites are smoother than those of orangeites (Fig. 7a), and their quenched-glassy and xenocryst-poor nature provides a closer match to primary liquid compositions. Kapamba lamproite trace element patterns partly resemble those of the most enriched high-Ti picrite lavas from the northern Karoo LIP in Botswana and Zimbabwe, whereas they are notably different from those of the low-Ti basalts from the same region (Fig. 7b). In general, the lamproites are characterized by very high LREE/HREE typical for primitive low-volume alkaline melts, in contrast

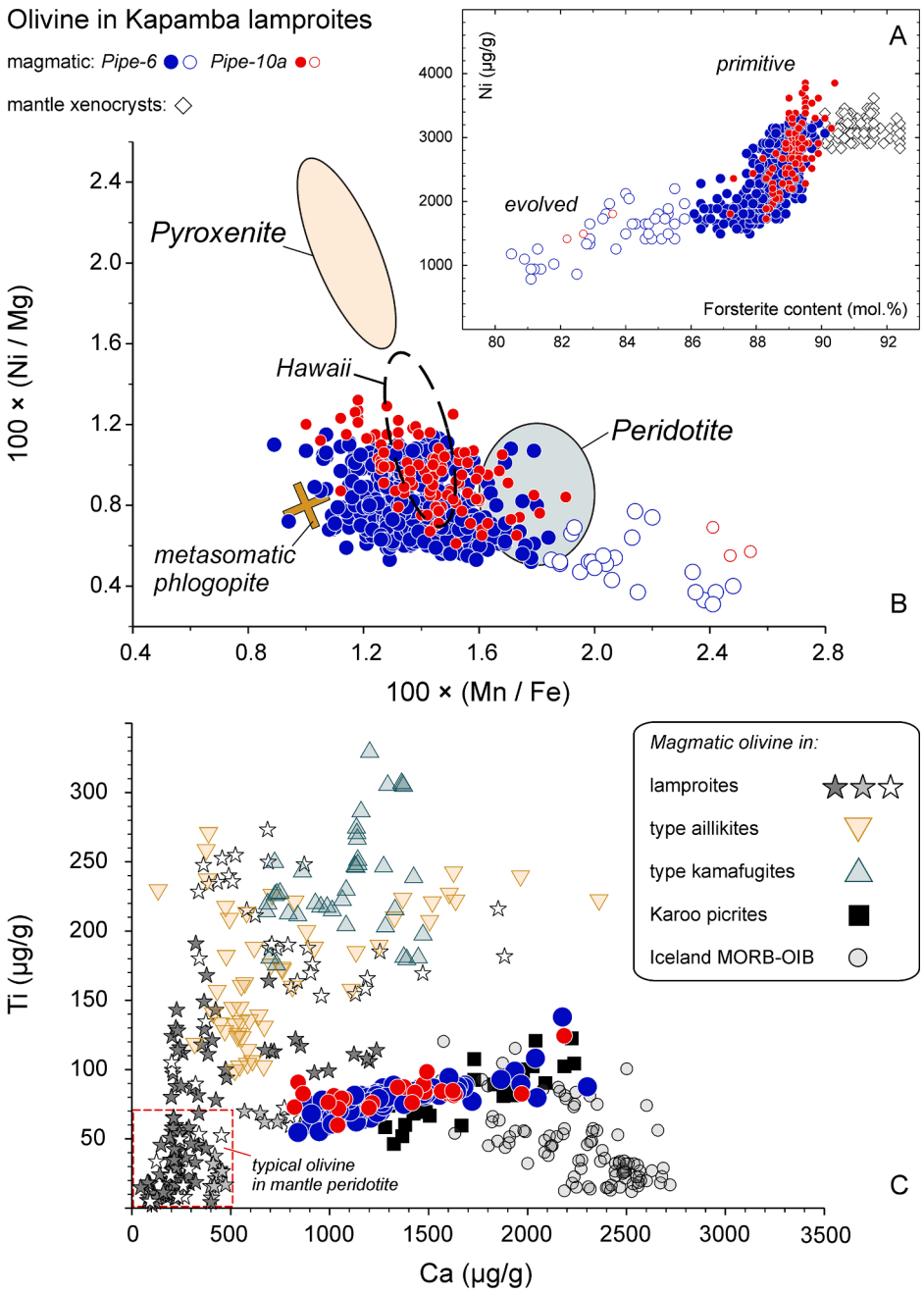


**Fig. 5.** EPMA- and LA–ICP–MS-determined olivine compositions in Kapamba lamproite Pipe-6 and Pipe-10a **(A-C)**. **(A)** The Ni *versus* forsterite systematics aid in distinguishing between cratonic mantle-derived xenocrysts (Ngwenya and Tappe, 2021) and magmatic crystal populations (this study), either as 'primitive' cores of, or 'evolved' overgrowths on, olivine microphenocrysts. **(B)** The Ni/Mg *versus* Mn/Fe ratios of olivine microphenocrysts in the Kapamba lamproites suggest melt derivation from a peridotite-dominated mantle source that contained significant metasomatic phlogopite, but only minor or no pyroxenite components. Compositional fields for endmember melts sourced from peridotite or pyroxenite, as well as for olivine phenocrysts from Hawaiian basalts are adopted from Sobolev et al. (2007). The metasomatic phlogopite endmember composition is taken from Veter et al. (2017). **(C)** The Ti *versus* Ca systematics of magmatic olivine from the Kapamba lamproites show strong Ca enrichment at moderately elevated Ti contents, similar to olivine phenocrysts in picrites from the Karoo LIP of southern Africa (Howarth and Harris, 2017). These minor and trace elements are also useful for distinguishing between magmatic olivine populations and peridotite-derived mantle xenocrysts (red dashed box; Foley et al., 2013). Note that olivine microphenocrysts in the Kapamba lamproites have significantly lower Ti contents than the olivine phenocrysts in type kamafugites from the East African Rift System and in lamproites from the West African craton, which are compositionally more similar to olivine phenocrysts in type aillikites from the rifted North Atlantic craton. Olivine data sources: dark grey stars, West Kimberley cratonic lamproites in Australia (Jaques and Foley, 2018); light grey stars, Mediterranean realm orogenic lamproites (Prelevic et al., 2013, Ammannati et al., 2016); open stars, West African cratonic lamproites (Howarth and Giuliani, 2020); type aillikites (Veter et al., 2017); type kamafugites (Foley et al., 2011); Karoo LIP picrites (Howarth and Harris, 2017); Iceland MORB–OIB (Rasmussen et al., 2020).

to the lower LREE/HREE recorded by higher-volume picritic magmas (Jourdan et al., 2007; Turunen et al., 2019). Although cratonic lamproite suites typically display a wide range of incompatible element patterns owed to complex mantle sources (Nelson et al., 1986), the Kapamba samples show trace element systematics that are broadly similar to those of lamproite suites from the East Antarctica portion of former Gondwanaland (Kjakebeinet and Gaussberg). These 'Gondwanan' lamproites reveal marked differences to other anorogenic lamproite suites, such as those from the Leucite Hills in western North America, which show stronger Th–U–Pb enrichments and notably more depleted Zr–Hf–Yb contents (Fig. 7c).

### 3.3.2. *Sr–Nd–Hf–Pb isotopic compositions*

The initial Sr, Nd, Hf and Pb isotopic compositions of the Kapamba lamproites are calculated for a magma emplacement age of 180 Ma (Supplementary Material). The initial $^{87}Sr/^{86}Sr$ ratios for all samples from the three lamproite pipes studied (Pipe-1, -6, -10a) are elevated ranging between 0.70701 and 0.70855, with most values clustering at around 0.7071. The range displayed by the corresponding $^{143}Nd/^{144}Nd$ values is very narrow, with subchondritic initial εNd values between −10.8 and −10. Only the sample from Pipe-1 shows a slightly higher εNd value of −8.1. In general, the initial Sr–Nd isotopic compositions of the Kapamba lamproites fall within the range of Kaapvaal craton orangeites and MARID xenoliths *(mica–amphibole–rutile–ilmenite–diopside)*, and they are slightly more enriched than the northern Karoo LIP picrites and basalts of high-Ti affinity (Fig. 8a). The Kapamba lamproites display a narrow range of $^{176}Hf/^{177}Hf$ ratios, with subchondritic initial εHf values between −20.3 and −19.1, similar to the most enriched members of the Kaapvaal craton orangeite and MARID xenolith suites (Fig. 8b).

The Kapamba lamproites show a restricted range in Pb isotope space (Fig. 9) with relatively low $^{206}Pb/^{204}Pb$ (16.8–17.5) at elevated

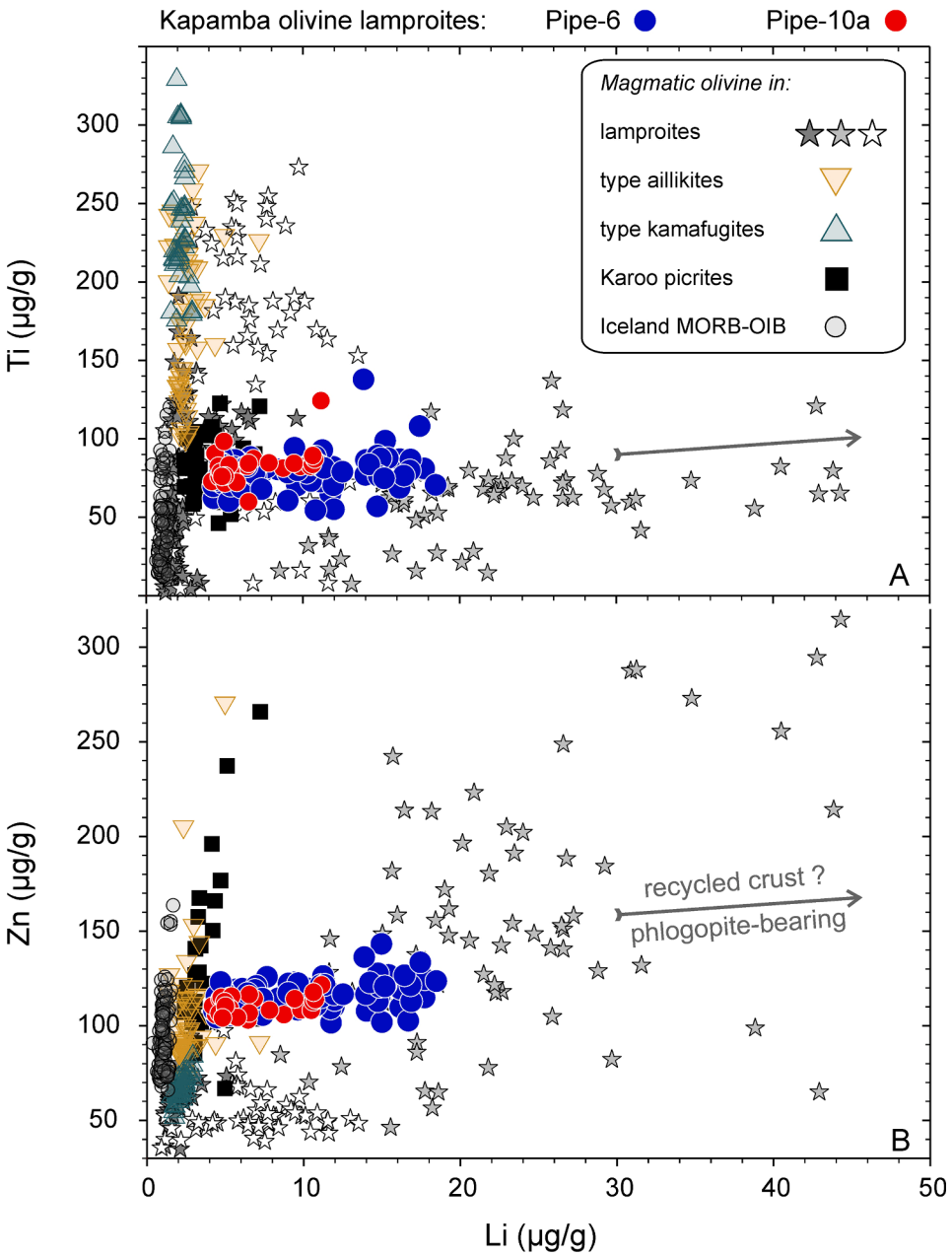


**Fig. 6.** LA–ICP–MS-determined olivine trace element compositions in Kapamba lamproite Pipe-6 and Pipe-10a **(A-B)**. **(A)** The Ti *versus* Li concentrations show a similar trend to olivine in Mediterranean realm orogenic lamproites, with marked Li enrichment at near-constant Ti. **(B)** The Zn *versus* Li concentrations also follow the olivine trend of Mediterranean lamproites, which was interpreted as a geochemical fingerprint of phlogopite melting in lithospheric mantle sources enriched in recycled crust components (Foley et al., 2013). Note the lower Zn concentrations for olivine microphenocrysts in the Kapamba lamproites compared to the olivine phenocrysts in picrites from the Karoo LIP of southern Africa (Howarth and Harris, 2017), which provides additional evidence against significant melt contributions from pyroxenite components beneath the Luangwa Rift structure (see Fig. 5b). Olivine data sources: dark grey stars, West Kimberley cratonic lamproites in Australia (Jaques and Foley, 2018); light grey stars, Mediterranean realm orogenic lamproites (Prelevic et al., 2013, Ammannati et al., 2016); open stars, West African cratonic lamproites (Howarth and Giuliani, 2020); type aillikites (Veter et al., 2017); type kamafugites (Foley et al., 2011); Karoo LIP picrites (Howarth and Harris, 2017); Iceland MORB–OIB (Rasmussen et al., 2020).

$^{207}Pb/^{204}Pb$ (15.5–15.6) and $^{208}Pb/^{204}Pb$ (37.1–37.6), similar to Kaapvaal craton orangeites and MARID xenoliths at their low $^{206}Pb/^{204}Pb$ ends. They also resemble the Pb isotopic compositions of several northern Karoo LIP flood volcanic units, especially those of the high-Ti picrites (Fig. 9a). The combination of low $^{206}Pb/^{204}Pb$ and high $^{207}Pb/^{204}Pb$, to the left of the present-day geochron, is characteristic for cratonic lamproites worldwide (Fig. 9b).

### 3.3.3. *Lithium isotopic compositions*

The Kapamba lamproites have $\delta^7Li$ values between +0.07 and +5.67‰ at elevated Li concentrations from 17 to 92 ppm (Supplementary Material). However, there are differences in the Li systematics for the samples from Pipe-6 and Pipe-10a. Five samples from Pipe-6 show a Li concentration range between 17.1 and 21.4 ppm at $\delta^7Li$ values between +2.80 and +5.67‰ (KP18-66 with 28.9 ppm Li and +0.07‰ $\delta^7Li$ represents an outlier; Fig. 10). In contrast, the five samples analyzed from Pipe-10a have much higher Li concentrations (47.4–92 ppm) at systematically lower $\delta^7Li$ (+1.65 to +2.25‰). Given that the samples from both pipes have identical Sr–Nd–Hf–Pb isotopic compositions (Figs. 8-9), and the fact that Pipe-6 yielded more pristine material than Pipe-10a (Ngwenya and Tappe, 2021), the Li systematics of Pipe-10a samples appear to be disturbed by secondary processes. Interactions between mantle-derived volcanic rocks and brine fluids in sedimentary basins may increase the Li concentrations and decrease $\delta^7Li$ (Araoka et al., 2014), as inferred for Pipe-10a volcanic rocks (Fig. 10). The spread in $\delta^7Li$ values displayed by the most pristine lamproite samples from Kapamba Pipe-6 is relatively small (+2.8 to +5.7‰ $\delta^7Li$) and firmly within the $\delta^7Li$ range of modern oceanic basalts and Archean to modern carbonatites (Halama et al., 2008; Krienitz et al., 2012; Tomascak et al., 2016). Although probably shifted by secondary processes to lower $\delta^7Li$ values, the less pristine Pipe-10a lamproite samples also fall within the mantle range (Fig. 10).

## 4. Significance of lamproites as part of the Karoo LIP

Mantle-derived ultrapotassic magmas have complex origins and can

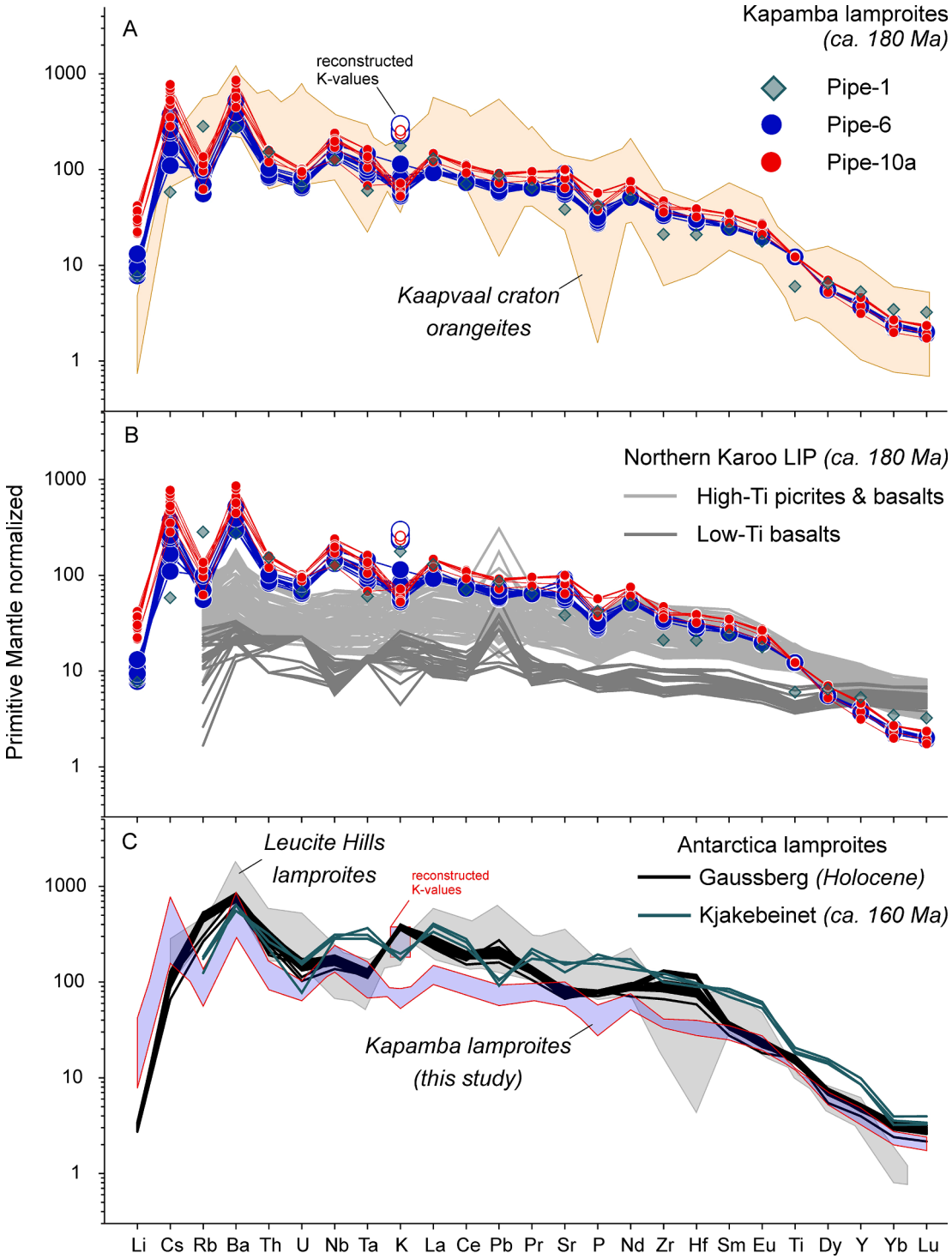


**Fig. 7.** Primitive mantle normalized incompatible element distributions for lamproite lavas from Kapamba Pipe-1, Pipe-6 and Pipe-10a, using the reconstructed K-concentrations of Ngwenya and Tappe (2021). **(A-C)** Comparison of the Kapamba lamproite trace element patterns with those of **(A)** magmatic Group-2 kimberlites (type orangeites) from the Kaapvaal craton in South Africa (Becker and le Roex, 2006; Tappe et al., 2022), **(B)** various flood volcanic units from the northern Karoo LIP in Botswana–Zimbabwe (Jourdan et al., 2007), and **(C)** lamproites from Gaussberg (Murphy et al., 2002) and Kjakebeinet (Luttinen et al., 2002) in East Antarctica, as well as from the classic Leucite Hills lamproites in western North America (Mirnejad and Bell, 2006). Primitive mantle values for normalization are taken from Palme and O'Neill (2003).

be generated over wide pressure ranges in diverse tectonic settings; for instance, at shallow mantle depths along active convergent plate margins, or much deeper beneath thick continental shields (Nelson et al., 1986; Foley, 1992; Prelevic et al., 2013). The observation that lamproite magmatism, sourced from the diamond stability field beneath a cratonic rift, is spatiotemporally linked to the Karoo LIP is unusual, and provides opportunities to further explore lamproite magma origins (Section 4.1) and to assess plume–lithosphere interaction as a mechanism by which metasomatic components are remobilized (Section 4.2), with potential climatic consequences.

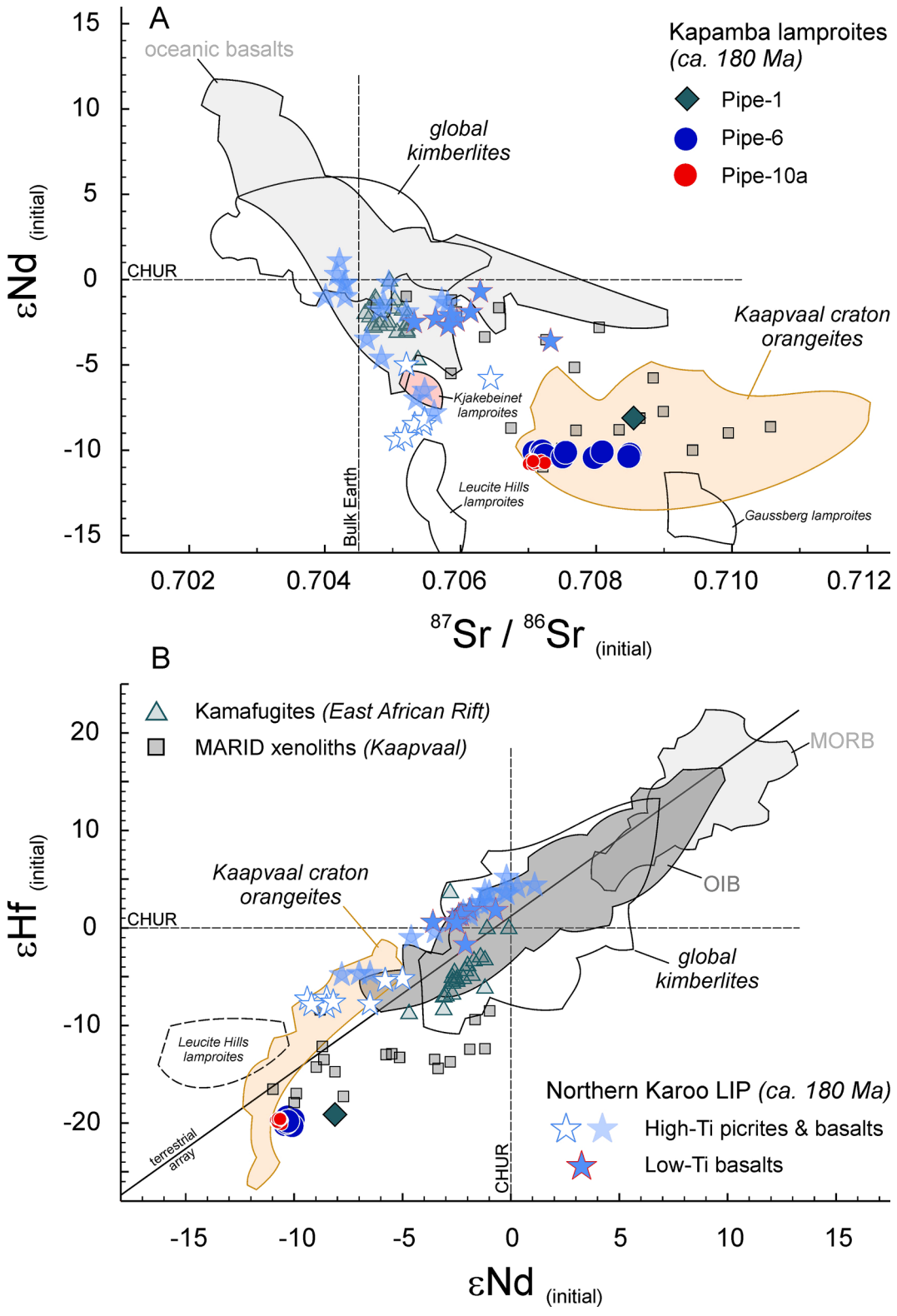


**Fig. 8.** Initial εNd *versus* $^{87}Sr/^{86}Sr$ **(A)**, and initial εHf *versus* εNd **(B)** for lamproite lavas from Kapamba Pipe-1, Pipe-6 and Pipe-10a in the Luangwa Rift structure of south-central Africa. Literature data sources: modern oceanic basalts, MORB and OIB (Stracke, 2012); volcanic–subvolcanic units of the northern Karoo LIP in Botswana–Zimbabwe (Jourdan et al., 2007); global kimberlite compilation (Tappe et al., 2020, and references therein); Kaapvaal craton Group-2 kimberlites, type orangeites (Fraser et al., 1985; Becker and le Roex, 2006; Tappe et al., 2022, and additional references therein); Kaapvaal craton MARID xenoliths (Fitzpayne et al., 2019b); type kamafugites from the East African Rift System (Rosenthal et al., 2009); Kjakebeinet lamproites, East Antarctica (Luttinen et al., 2002); Gaussberg lamproites, East Antarctica (Murphy et al., 2002); Leucite Hills lamproites, Wyoming (Mirnejad and Bell, 2006, and references therein). The parameters applied in age corrections, calculations of 'epsilon' notations, and Nd–Hf isotope array projections are summarized in the Supplementary Material.

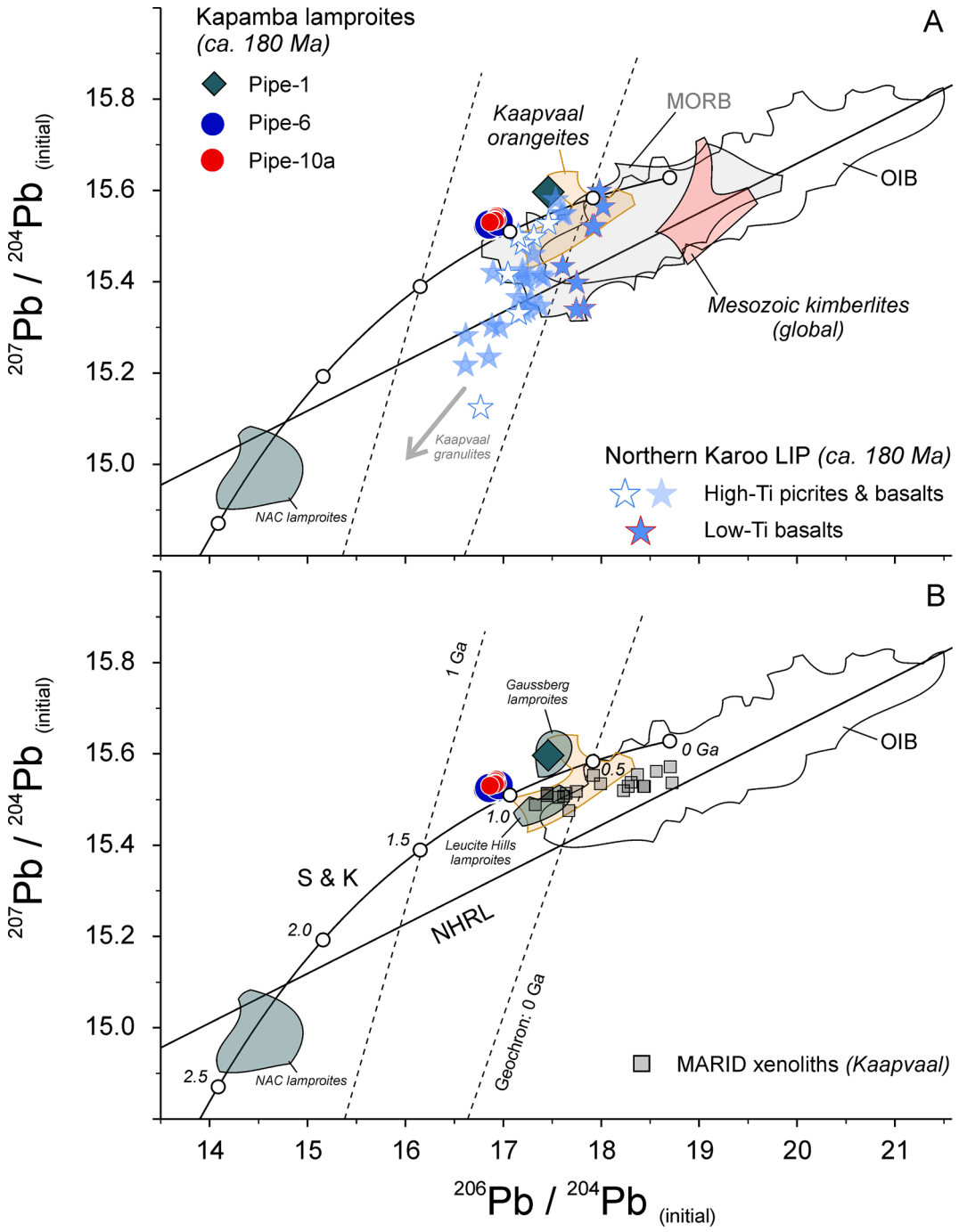


**Fig. 9.** Initial $^{207}Pb/^{204}Pb$ *versus* $^{206}Pb/^{204}Pb$ for lamproite lavas from Kapamba Pipe-1, Pipe-6 and Pipe-10a in the Luangwa Rift structure of south-central Africa **(A-B)**. The vector towards 'Kaapvaal granulites' serves as a proxy for the Pb isotopic compositions of Precambrian basement rocks in sub-Saharan Africa (Huang et al., 1995), indicating crustal contamination of some Karoo flood basalt units **(A)**. Literature data sources: modern oceanic basalts, MORB and OIB (Stracke, 2012); volcanic–subvolcanic units of the northern Karoo LIP in Botswana–Zimbabwe (Jourdan et al., 2007); global Mesozoic kimberlites (Tappe et al., 2017, and references therein); Kaapvaal craton Group-2 kimberlites, type orangeites (Fraser et al., 1985, and references therein); Kaapvaal craton MARID xenoliths (Fitzpayne et al., 2019b); Gaussberg lamproites, East Antarctica (Murphy et al., 2002); Leucite Hills lamproites, Wyoming (Mirnejad and Bell, 2006); NAC lamproites, Greenland–Labrador (Tappe et al., 2007, and references therein). The Stacey–Kramers (S&K) terrestrial Pb isotope evolution curve is shown for reference, with time-steps denoted in 0.5-billion-years increments. 'Geochron' positions were calculated for present-day (0 Ga) and 1 Ga, using a 4.55 Ga age of Earth with an initial Pb isotopic composition proxied by the Canyon Diablo troilite. NAC – North Atlantic Craton; NHRL – Northern Hemisphere Reference Line.

### 4.1. *Origin of ca. 180 Ma lamproites beneath the failed Luangwa Rift*

#### 4.1.1. *Olivine evidence for a phlogopite-rich peridotitic mantle source*

Combined major and trace element datasets for magmatic olivine hold clues to source-forming processes in the upper mantle, including changes in the mineralogy and redox state of the rock types involved in melt generation (Foley et al., 2013). At Kapamba, the most primitive olivine microphenocrysts (90–86 mol.% forsterite; Fig. 5a) have relatively low Ni/Mg and Mn/Fe ratios (Fig. 5b), which suggests that the lamproite melts were sourced from peridotitic mantle with a notable modal phlogopite metasomatic overprint (Veter et al., 2017). The low Ni/Mg ratios rule out significant melt contributions from pyroxenitic

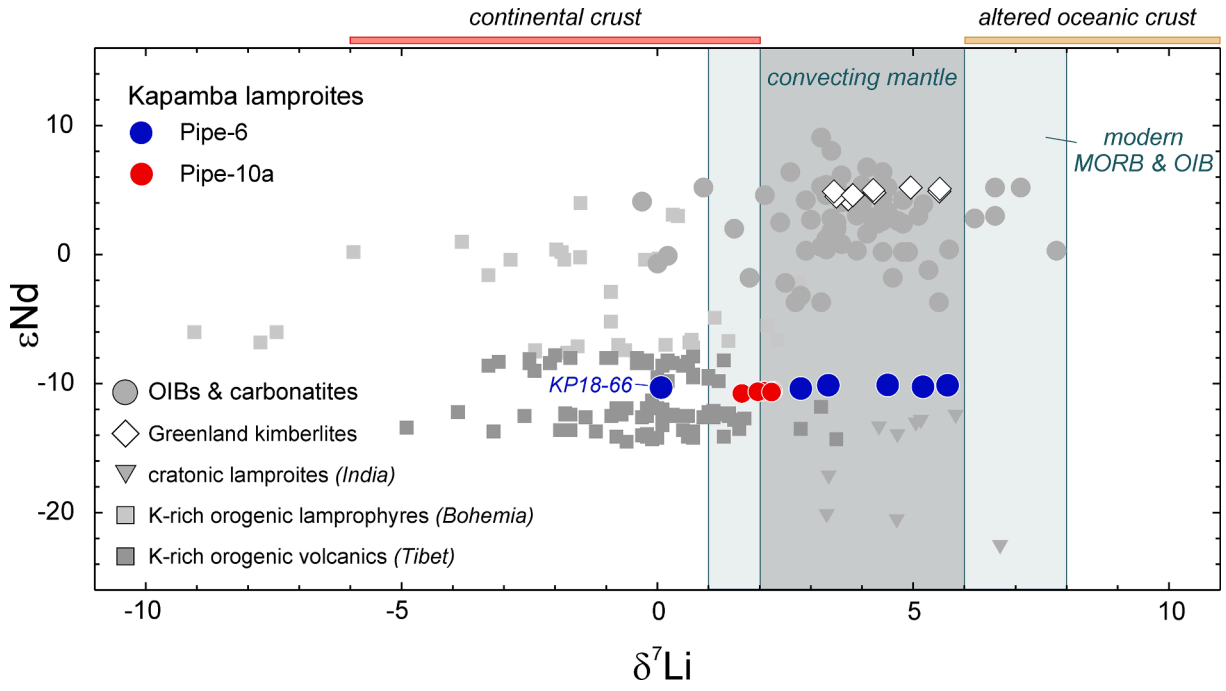


**Fig. 10.** Initial εNd *versus* $\delta^7$Li for lamproite lavas from Kapamba Pipe-6 and Pipe-10a in the Luangwa Rift structure of south-central Africa. The positions of selected geochemical reservoirs are adopted from Tomascak et al. (2016) and Krmíček et al. (2022). Literature data sources: modern oceanic basalts, MORB and OIB (Krienitz et al., 2012; Tomascak et al., 2016); modern to Archean carbonatites (Halama et al., 2008); Greenland kimberlites (Tappe et al., 2017); cratonic lamproites from India (Krmíček et al., 2022); post-collisional K-rich mafic rocks from the Bohemian Massif and Tibetan Plateau (Krmíček et al., 2020; Tian et al., 2020).

components (Sobolev et al., 2007), considered previously as an important mantle source lithology in global lamproite magma genesis (Foley, 1992). However, Heinonen and Fusswinkel (2017) pointed out that the effects of pressure–temperature–$H_2O$ on Ni–Mn in olivine can overcome the mineralogical control. These authors reasoned that source mineralogy and thus lithology can only be distinguished for primitive volcanic rocks that formed under similar conditions, such as diverse suites of cratonic mantle-derived lavas.

The Ca–Ti systematics of the most primitive magmatic olivine population from the Kapamba lamproites resemble those of olivine phenocrysts in Karoo LIP picrite lavas and sills from the Tuli and Mwenezi basins in Zimbabwe, some 800 km farther south (Howarth and Harris, 2017) (Fig. 5c). However, lamproitic olivine from the Luangwa Rift has much higher Li (4.2–18.5 ppm) and significantly lower Zn (102–143 ppm) abundances than olivine from the Zimbabwean picrites (Fig. 6). This suggests contrasting roles for phlogopite-enriched (high-Li) and clinopyroxene-enriched (high-Zn) minor components within heterogeneous, yet peridotite-dominated, cratonic mantle sources beneath southern Africa. The Li enrichment of Kapamba olivine resembles that observed for olivine phenocrysts from many Alpine–Himalayan lamproite occurrences (Fig. 6). In this orogenic setting, newly-accreted refractory shallow mantle lithosphere was refertilized by melts/fluids derived from spatially-associated recycled sediment in a subduction zone mélange environment (Prelevic et al., 2013). Although it is tempting to ascribe the Li enrichment in olivine from the anorogenic Kapamba lamproites to involvement of recycled sediment at great mantle depths, it must be noted that this Li enrichment is not as extreme as observed for olivine in much shallower-sourced orogenic lamproites (Krmíček et al., 2016). Subducted crustal Li is not expected to enter the deeper convecting mantle, as evident from exclusively mantle-like $\delta^7$Li compositions in the global OIB record (Krienitz et al., 2012) (Fig. 10), and from the low Li contents in magmatic olivine from kimberlites (Howarth et al., 2022). In orogenic lamproites, extreme Li enrichment in olivine is typically coupled to strong Zn enrichment, which is not observed at Kapamba (Fig. 6b). Zinc in magmatic olivine is an additional trace metal that potentially indicates involvement of subducted carbonate-bearing sediment during refertilization of peridotitic mantle, with clinopyroxene-forming decarbonation reactions as the main metal transfer mechanism (Ammannati et al., 2016).

Comparison of olivine compositions from carbonate-free ultrapotassic magmas (e.g., Kapamba lamproites) and from K-rich carbonated silicate melts (i.e., type kamafugites and aillikites), all emplaced in cratonic rift environments, reveals that the lamproites have significantly higher Li at much lower Ti contents, but similarly low Zn concentration levels (Fig. 6). This observation supports the idea of contrasting metasomatic styles, without involvement of recycled marine carbonates, during preconditioning of the lithospheric mantle sources of anorogenic lamproites and K-rich carbonated silicate magmas (Tappe et al., 2008).

In short, the olivine trace and minor element compositions (elevated Li at low Mn/Fe and Ni/Mg) of the anorogenic lamproites from Kapamba point to phlogopite-rich mixed peridotitic source assemblages, but it remains to be discussed whether recycled continent-derived sediment contributed to lithospheric mantle enrichment.

#### 4.1.2. *Isotope evidence against recycled sediment in the cratonic mantle source*

The most pristine Kapamba lamproite samples exhibit a relatively small range of $\delta^7$Li values between +2.8 and +5.7‰, closely matching the global mean for mantle-derived magmas between +3 and +5‰ (Krienitz et al., 2012; Tomascak et al., 2016). They also overlap with the Li isotopic compositions of cratonic lamproites from India (Krmíček et al., 2022) and kimberlites from Greenland (Tappe et al., 2017), which exhibit $\delta^7$Li values within the mantle range (Fig. 10). In contrast, the shallower-sourced orogenic K-rich mafic rocks from Phanerozoic mountain belts in Europe and Asia have much lower $\delta^7$Li compositions, mostly scattering around zero but also down to −5‰ (Krmíček et al., 2020; Tian et al., 2020). The Li isotopic signatures of these orogenic mantle-derived potassic rocks are compatible with LILE enrichments caused by recycled continental crust, probably in the form of subducted sediment (−6 to +2‰ $\delta^7$Li; Fig. 10). Although the global Li isotope database for potassic rocks and kimberlites is relatively small, it appears that recycled sediment signatures are common in magmatic provinces

that formed near 'active' convergent plate margins, whereas they are rarely observed in deeper-sourced magmatic suites on and around cratons, where any influence by subduction was either spatially or temporally distant (Fig. 10).

The contrasting styles of lithospheric mantle source enrichment revealed by the Li isotopic compositions of orogenic and anorogenic lamproites (and related magmas) are not always mirrored by their radiogenic isotope compositions. Both orogenic and anorogenic lamproite suites from occurrences worldwide exhibit some of the strongest Sr–Nd–Hf–Pb isotopic enrichments measured for mantle-derived igneous rocks (Nelson et al., 1986; Davies et al., 2006; Tappe et al., 2007), and the cratonic lamproites at Kapamba are no exception (Figs. 8-9). Such strong mantle source enrichment can be attained in two principle ways: *(1)* fairly recent addition of incompatible elements from metasomatic agents that contain an ancient component, such as Precambrian sediment (Murphy et al., 2002; Prelevic et al., 2010), or *(2)* incompatible element addition from mantle-derived low-degree melts or fluids, without contributions from recycled sediment, billions of years ago (Davies et al., 2006; Mirnejad and Bell, 2006; Tappe et al., 2007).

The Sr–Nd–Hf–Pb isotopic compositions of the Kapamba lamproites resemble those of certain Kaapvaal craton orangeites and MARID xenoliths (Figs. 8-9), for which no involvement of recycled sedimentary components has been advocated, based on radiogenic and $\delta^{15}N$–$\delta^{18}O$–$\varepsilon^{205}Tl$ stable isotope evidence (Fitzpayne et al., 2019a; Fitzpayne et al., 2019b; Fitzpayne et al., 2020). Any crustal fingerprint detected in these cratonic mantle derived K-rich rocks probably originates from fluids released from recycled igneous oceanic crust (Fitzpayne et al., 2020), which is a common enriched component within the convecting mantle (Stracke, 2012). However, the association of highly unradiogenic Nd with anomalous Pb isotopic compositions, with elevated $^{207}Pb/^{204}Pb$ at low $^{206}Pb/^{204}Pb$ to the left of the present-day geochron, may record a contribution of ancient continent-derived sediment in a putative ultradeep sublithospheric mantle source for the modern Gaussberg lamproites in East Antarctica (Murphy et al., 2002). Although the Kapamba lamproites have similar isotopic and trace elemental traits (e.g., ZK1-1 from Pipe-1; Figs. 8-9), they do not exhibit the positive Pb anomaly in normalized abundance diagrams (Fig. 7), which is considered a hallmark feature of mantle-derived magmas from sources that contain significant recycled sediment (Prelevic et al., 2010). Furthermore, the Kapamba lamproites lack negative Ti–Nb–Ta anomalies characteristic for mantle-derived K-rich magmas erupted at or near active convergent plate margins (Foley and Wheller, 1990; Lustrino et al., 2019), and the relative depletion in Th–U argues against recycled continent-derived sediment in their mantle source (Plank, 2014). In general, the elemental and isotopic compositions of lamproites from Kapamba Pipe-6 and Pipe-10a in the Luangwa Rift are compatible with magma origins from long-term enriched K-metasomatized cratonic mantle lithosphere, without significant contributions from recycled sediment. The fact that Mesozoic–Cenozoic anorogenic lamproites (and orangeites) across former Gondwanaland, including the Gaussberg volcano, have broadly similar incompatible trace element and radiogenic isotope compositions (Figs. 7-9) supports ultrapotassic magma origins from similarly metasomatized regional lithospheric mantle domains (Nelson et al., 1986; Luttinen et al., 2002; Becker and le Roex, 2006; Giuliani et al., 2015; Tappe et al., 2022), rather than invoking geochemical reservoirs within the deep convecting mantle (Murphy et al., 2002; Liu et al., 2022).

#### 4.1.3. Constraints on the timing of phlogopite-rich mantle metasomatism

MARID-type metasomes within deep lithospheric roots are viable source components to lamproite, ultramafic lamprophyre and orangeite magmatism in cratonic regions (Foley, 1992; Tappe et al., 2008; Giuliani et al., 2015), but also on thick oceanic plateaus (Smart et al., 2019). The close Sr–Nd–Hf–Pb isotopic match between MARID xenoliths from the Kaapvaal craton (Grégoire et al., 2002; Fitzpayne et al., 2019b) and the Kapamba lamproites supports this relationship for cratonic sub-Saharan Africa. For the Kapamba lamproites, our geochemical data (Section 4.1.1 and 4.1.2) suggest that such a phlogopite-rich peridotitic mantle source formed by the addition of incompatible elements from low-degree partial melts of the underlying asthenosphere, and that the strong isotopic enrichment developed by radiogenic in-growth within the isolated lithosphere. This model is similar to the concept developed by McKenzie (1989) to explain small K-rich melt fractions in the asthenosphere and their capacity to infiltrate into and freeze within the lower lithospheric mantle, where remobilization due to extensional tectonics or plume activity can trigger potassic magmatism.

To test this model, we calculated the possible range of Nd–Hf isotopic compositions for natural MARID materials back to 2 Ga, applying the full range of known present-day parent–daughter isotope ratios (Fitzpayne et al., 2019b), and assuming a BSE-like isotopic 'starting' composition for the asthenosphere-derived metasomatic agent (εNd–εHf at zero; Fig. 11b). These calculations suggest that the inferred MARID-type metasomatic component beneath the cratonic Luangwa Rift was approximately 1 Ga old when tapped by lamproite magmatism at ca. 180 Ma (Fig. 11b). The application of a more enriched isotopic starting composition relative to Bulk Earth would necessitate shorter residence times of less than one billion years, but such strongly enriched components are very rare in the asthenosphere and therefore unlikely to play an important role in lithospheric mantle metasomatism. On the other hand, metasomatic reaction experiments across redox boundaries at pressure–temperature conditions of the lowermost cratonic mantle show that percolating carbonated silicate melts, akin to asthenosphere-derived kimberlitic liquids, can produce MARID assemblages near the lithosphere–asthenosphere boundary (Pintér et al., 2022). Recent investigations of MARID xenoliths from the Kaapvaal craton also suggest a role for kimberlitic mantle metasomatism in their formation (e.g., Fitzpayne et al., 2018). To account for isotopically more depleted kimberlitic metasomatic agents, we calculated mantle residence times for MARID materials using the Nd–Hf isotopic compositions of Mesozoic–Cenozoic kimberlites from sub-Saharan Africa (Tappe et al., 2020). This scenario prolongs the residence times slightly, to approximately 1.0–1.2 Ga (Fig. 11b). Strontium isotope constraints on these petrogenetic models are challenging because of the extremely wide Rb/Sr range (<0.5 to >2) exhibited by natural MARID materials (Grégoire et al., 2002; Fitzpayne et al., 2018; Smart et al., 2019). Only the application of the lowest measured $^{87}Rb/^{86}Sr$ ratios for certain bulk cratonic MARID xenoliths (~0.4; Grégoire et al., 2002), with ≤45 vol% phlogopite, corroborates lithospheric mantle residence times of around one billion years (Fig. 12).

The calculations presented above demonstrate that the Kapamba lamproites may originate from MARID-style metasomatized 'mixed' peridotitic mantle lithosphere (that contained up to a few modal-% phlogopite), with a major period of source preconditioning at around 1 Ga (Figs. 11-12). The inferred timing of mantle metasomatism is broadly coeval with Mesoproterozoic continental collisions during which the Irumide Belt formed in between the Congo–Tanzania and Kalahari cratons (De Waele et al., 2006) (Fig. 2). Isotopic dates of around 1 Ga have also been reported for peridotite xenoliths ($^{40}Ar/^{39}Ar$ phlogopite; note that the K–Ar system in phlogopite can remain closed in upper mantle environments to above 1000 °C; Hopp et al., 2008) sampled along the Kaapvaal craton margins, and they may record a discrete metasomatic event that affected the lithospheric mantle during the Mesoproterozoic Namaqua–Natal orogeny in southern Africa (Hopp et al., 2008). Collectively, these Mesoproterozoic collisional events in sub-Saharan Africa were part of Rodinia supercontinent formation, and the widely recognized mantle metasomatic overprint at this time can be explained by creation of additional new melt/fluid pathways within the lowermost cratonic lithosphere in response to increased plate-tectonic stresses (Tappe et al., 2018). Melt/fluid ingress from the asthenosphere into the lowermost lithosphere during the Mesoproterozoic, without significant contributions from recycled sediment, is supported by the fact that the initial $^{206}Pb/^{204}Pb$ ratios of the metasome-sourced Kapamba lamproites

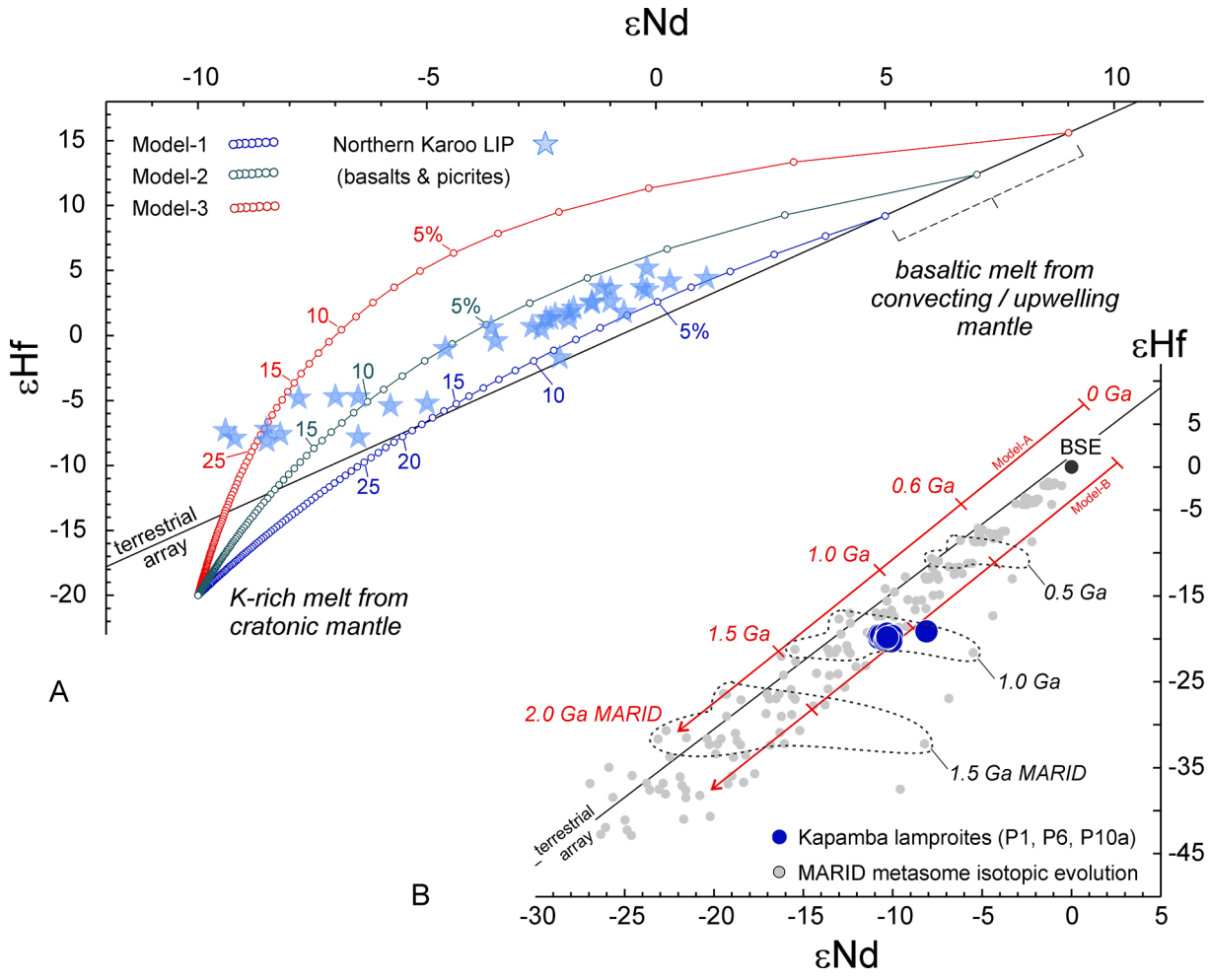


**Fig. 11.** The initial εHf versus εNd diagrams **(A-B)** explore possible source-forming processes and magma evolution trajectories for the petrogenesis of coeval cratonic lamproites (this study) and flood basalts/picrites (Jourdan et al., 2007) within the ca. 180 Ma northern Karoo LIP. The modelling in **Panel A** shows two-component mixing between basaltic melts from the convecting or upwelling mantle and K-rich hydrous silicate melts of lamproitic affinity from the continental lithospheric mantle (i.e., fusion melting; the Supplementary Material provides a summary of the endmember parameters; mixing increments in 1%-steps). Three scenarios are explored: In Model-1, strongly enriched lamproitic melt (using Kapamba elemental and isotopic compositions) is mixed into moderately depleted basaltic melt from a sublithospheric source (using low-Ti Karoo basalt elemental and 'accessible' upper mantle isotopic compositions). In Model-2, strongly enriched lamproitic melt (using global average cratonic lamproite elemental and Kapamba lamproite isotopic compositions) is mixed into depleted basaltic melt from a sublithospheric source (using low-Ti Karoo basalt elemental and average 'accessible' upper mantle isotopic compositions). In Model-3, strongly enriched ultrapotassic melt (using extreme East African Rift kamafugite elemental and Kapamba lamproite isotopic compositions) is mixed into strongly depleted basaltic melt from a sublithospheric source (using low-Ti Karoo basalt elemental and 'accessible' upper mantle isotopic compositions). The modelling in **Panel B** constrains the age and origin of MARID-type metasomatic components within the cratonic mantle lithosphere beneath sub-Saharan Africa. The grey dots represent calculated model Nd–Hf isotopic compositions of MARID materials from the Kaapvaal craton back to 2 Ga, using the full range of known elemental concentrations (Fitzpayne et al., 2019b) and assuming an isotopic 'starting' composition of the metasomatic agent similar to BSE. The grey dashed outlines suggest that at these boundary conditions, the MARID-type metasomatic mantle component beneath the cratonic Luangwa Rift structure was approximately 1 Ga old. The calculations for *Model-A* and *Model-B* (red curves) also use Nd and Hf concentrations typical for MARID materials, but the isotopic 'starting' compositions (0 Ga) for the inverse modelling are set to those of moderately depleted Monastery and Igwisi Hills kimberlites, respectively (Tappe et al., 2020). Even with these modified assumptions, the inferred MARID-type component has an apparent age of 1.0–1.2 Ga.

(and Kaapvaal orangeites) fall to the right of the 1 Ga geochron in Pb isotope space (Fig. 9).

### 4.2. The case for plume–lithosphere interaction

#### 4.2.1. Rifting versus plume impingement in cratonic lamproite volcanism

Developing an understanding of the unconventional setting of ultrapotassic volcanism at Kapamba will provide new insights into rift tectonics and mantle plume impingement in regions characterized by thick lithosphere. Although the Kapamba lamproites are spatially associated with the down-faulted graben structures of this 60-km-wide cratonic rift, timing of magma emplacement at 178.1 ± 8.4 Ma is unrelated to the main phase of rifting between ca. 270 and 230 Ma, as evident from the well-preserved biostratigraphic record of Luangwa Valley (Angielczyk et al., 2014). Geophysical studies across the Luangwa Rift and adjoining branches in the region found that crustal stretching is very low in comparison to major continental rift structures worldwide (Wang et al., 2019). Furthermore, Sarafian et al. (2018) noted that the underlying lithospheric mantle was hardly affected by Permo–Triassic or Cenozoic rifting. These geophysical results agree with new petrological findings that demonstrate the presence of relatively cold cratonic lithosphere ($\leq$42 mW/m$^2$) down to at least 180 km depth at the time of lamproite volcanism (Ngwenya and Tappe, 2021). In general, the cratonic lithosphere provides a favorable environment for long-term storage of phlogopite-rich mantle metasomes, from mid-lithospheric depth (Aulbach et al., 2017) down to the lithosphere–asthenosphere

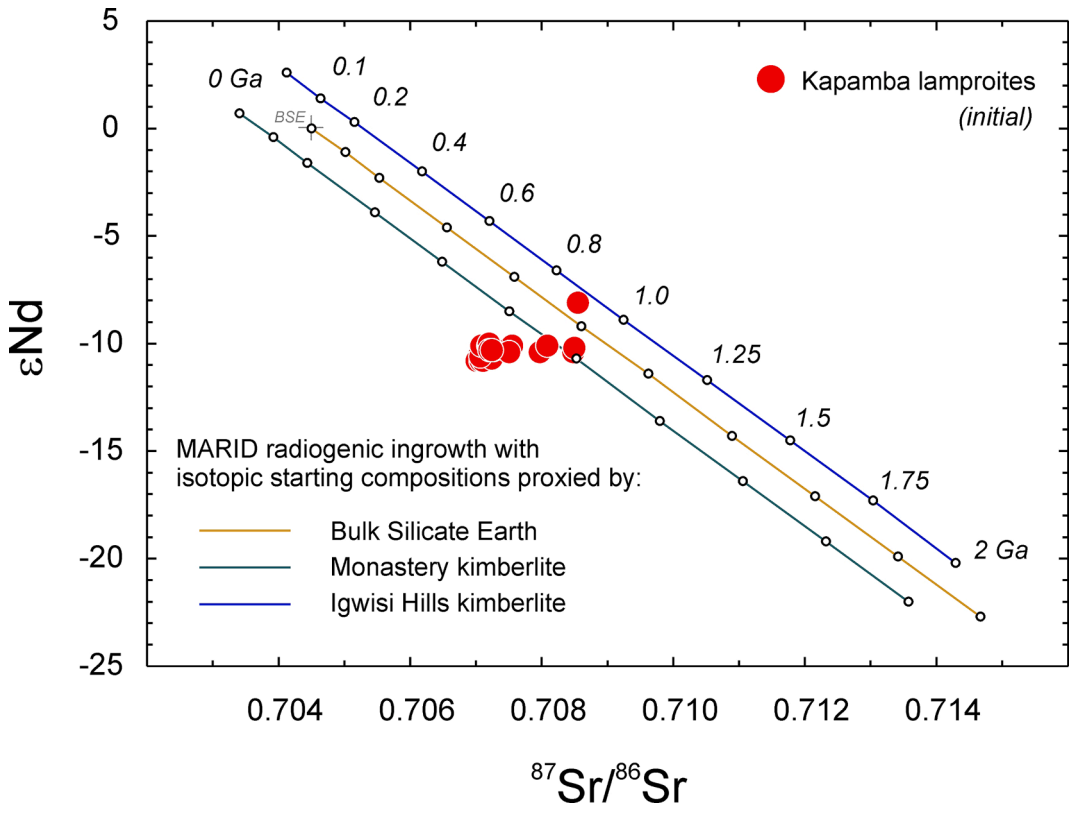


**Fig. 12.** A Sr–Nd isotope model for the age and origin of MARID-style mantle metasomatism beneath sub-Saharan Africa (model parameters are provided in the Supplementary Material). The ca. 180 Ma old Kapamba lamproites are compared with the calculated (model) Sr–Nd isotopic compositions of natural MARID material with ~45 vol% phlogopite back to 2 Ga, using a $^{87}Rb/^{86}Sr$ ratio of ~0.4 (Grégoire et al., 2002).

boundary well within the diamond stability field (Konzett et al., 1997; Pintér et al., 2022). Importantly, the style of rift tectonics that affected south-central Africa during the Phanerozoic, dominated by strike-slip and wrench-faulting, was unable to remobilize the ca. 1 Ga old phlogopite-rich metasomes inferred to be present in the regional cratonic mantle lithosphere (Fig. 11b). In analogy to most segments of the western branch of the East African Rift System (Rosenthal et al., 2009; O'Donnell et al., 2016; Rooney, 2020), the Luangwa Rift also remained amagmatic during its most active tectonic phase in Permo–-Triassic times.

The current best estimate of lamproite magma emplacement in Luangwa Valley at 178.1 ± 8.4 Ma coincides with the well-constrained age of the Karoo LIP in sub-Saharan Africa, where the majority of basaltic flood volcanism and sill emplacement occurred between 183 and 177 Ma (Greber et al., 2020) (Fig. 4c). The nearest inferred Karoo LIP feeder zone is the so-called Zambesi 'plume' centre some 200–400 km south of the Luangwa Rift in the border region between Zambia and Zimbabwe. These observations imply a genetic link between the Karoo LIP and ultrapotassic volcanism in sub-Saharan Africa (e.g., several early Jurassic orangeite pipes occur in southern Africa; Griffin et al., 2014; Tappe et al., 2018; Fig. 4c), and heat transfer from an arriving plume head beneath the Gondwanan lithosphere is a viable mechanism to locally fuse phlogopite-rich cratonic mantle peridotite, possibly aided by redox melting (Pintér et al., 2022). Temperature modelling demonstrates that the thermal effect of mantle plume head arrival (with >150 °C excess temperature) beneath continents is strongest for lithospheres with 160 to 190 km thickness (Ernst et al., 2018), comparable to the Luangwa Valley region in the northern vicinity of the suspected impingement site (Fig. 2).

Our case from sub-Saharan Africa adds to the growing list of examples in which low-volume alkaline and carbonatitic magmatism was intimately associated with LIP-sized mantle melting events (Ernst, 2014). Among the most relevant examples are the small carbonatite intrusions of Karoo LIP age in SE Zimbabwe (Harmer et al., 1998), but also K-rich diamondiferous orangeite magma eruptions in central India at ca. 65 Ma as part of the Deccan LIP event (Chalapathi Rao and Lehmann, 2011). LIP associated alkaline magmatic activity typically occurs at the periphery of mantle plume impingement sites beneath relatively thick continental lithospheres (Ernst, 2014). However, the position of the ca. 180 Ma Kapamba lamproites, well within the confines of the northern Karoo LIP (Fig. 1b), suggests ultrapotassic magma formation during cratonic mantle reactivation caused by emanating heat or push from an arriving plume head (e.g., McKenzie, 1989). Sublithospheric melt contributions to the cratonic mantle derived Kapamba lamproites, as proposed for other occurrences worldwide (O'Brien et al., 1995; Sarkar et al., 2022), appear to be absent given the lack of magmatic carbonates and isotopic mixing trends between enriched and depleted components (e.g., Tappe et al., 2008).

Impingement of the plume head at the underside of the Gondwanan cratonic lithosphere caused picritic and basaltic magma production only in significantly pre-thinned rift branches (e.g., Zambesi and Lebombo rifts), whereas the extent of lithosphere thinning beneath the failed Luangwa Rift remained insufficient for major melting to occur (Thompson and Gibson, 1991). Importantly, picritic and basaltic magmas sourced from the plume were likely to encounter K-rich cratonic mantle metasomes, as proxied by the ca. 180 Ma Kapamba lamproites. Magma-induced heat transfer into the otherwise difficult-to-melt cratonic mantle lithosphere would cause efficient scavenging of phlogopite-rich metasomatic domains. This process should leave an imprint on the incompatible element systematics, including their radiogenic isotope compositions, of some flood volcanic units (McKenzie, 1989).

#### 4.2.2. Implications for the geochemistry of continental flood basalts

The origin of enriched geochemical signatures in continental flood basalts remains contentious. While some workers demonstrated mafic magma contamination by the continental crust (Carlson et al., 1981; Arndt et al., 1993; Day et al., 2021), others argue for melt contributions from old metasomatic domains that were remobilized from the deepest continental lithosphere during mantle plume impingement (Ellam et al., 1992; Larsen et al., 2003; Giuliani et al., 2014). Some models suggest up to 50% melt contributions from such metasomatized mantle reservoirs to the plume-initiated flood volcanism, and these models also derive the frequently observed Ti-provinciality (high-Ti *vs* low-Ti) from variable melt contributions of lithospheric mantle sources (Gibson et al., 1996; Jourdan et al., 2007). For the northern Karoo LIP, it appears that the low-Ti basalts have generally much lower incompatible element contents (but stronger fingerprints of crustal contamination such as negative Nb and positive Pb anomalies) compared to the high-Ti basalts and picrites, which approach the very high LILE–LREE–HFSE concentration levels of the Kapamba lamproites (Fig. 7b). Therefore, it seems plausible that plume–lithosphere interactions played a role in the generation of voluminous high-Ti flood volcanic units, including alkali-rich picrites (e.g., Larsen et al., 2003), which are difficult to explain by low-degree mantle melting. We acknowledge, however, that low-degree partial melting of the convecting upper mantle beneath thick continental lithosphere can be a viable alternative in the formation of high-Ti flood basalts (e.g., Arndt et al., 1993).

To further explore the viability and extent of plume–lithosphere interactions, we performed two-component mixing calculations between basaltic melts from upwelling mantle *(plume)* sources, proxied by low-Ti Karoo basalts, and K-rich hydrous silicate melts from the continental lithospheric mantle, as proxied by the Kapamba lamproites (Fig. 11a). The Nd–Hf isotope model calculations suggest that the flood volcanic units of the northern Karoo LIP contain between 2 and 25% mass-fraction of K-rich melt component from metasomatized cratonic mantle lithosphere, admixed into passing plume-derived picritic to basaltic liquids (Fig. 11a). This finding supports earlier notions about limited involvement of the continental mantle lithosphere in flood basalt formation (1–15%), based on energy-constrained AFC modelling (Heinonen et al., 2016). However, our case from sub-Saharan Africa reinforces the argument that thick continental lithosphere cannot remain passive during mantle plume impingement and, in all likelihood, participates actively in the formation of LIPs.

#### 4.2.3. Possible influence of craton reactivation on climate change

Many studies argued that the most intensive biotic mass extinctions are associated with flood volcanism on and around cratons, in contrast to the more voluminous oceanic LIPs that tend to have a smaller environmental impact (for a recent review, readers are referred to Black et al., 2021). Using the Karoo LIP as an example, Guex et al. (2016) suggest that critical amounts of $SO_2$ were released into the atmosphere via early-stage alkaline magmatism, causing a short period of global cooling coincident with a biotic crisis. This precursory magmatic activity to the main phase of predominantly $CO_2$-emitting flood volcanism was sourced from volatile-enriched (e.g., sulphide-bearing) metasomatized cratonic mantle lithosphere, reactivated during plume impingement (Guex et al., 2016).

Although the case of the diamondiferous Karoo lamproites aligns with the tectonomagmatic model by Guex et al. (2016), the proposed link between craton reactivation and climate change is problematic, because the peridotite-dominated cratonic mantle lithosphere is on average not particularly more sulphur-rich than other mantle reservoirs (~300 ppm *vs* ~200 ppm S in the primitive mantle; Aulbach et al., 2016). The glassy, little-degassed Kapamba lamproites contain <500 ppm S, which suggests that even hydrous metasomatic portions of the cratonic mantle lithosphere are not very sulphur-rich. Indeed, MARID xenoliths from the Kaapvaal craton contain only 612 ± 557 ppm S on average (n = 11; Supplementary Material). Thus, in our plume–lithosphere interaction model for the Karoo LIP, craton reactivation is an improbable source of the excess $SO_2$ required to cause short-pulsed atmospheric cooling at the Pliensbachian–Toarcian boundary. Based on these findings, a thermogenic origin of the excess $SO_2$ is more likely (Svensen et al., 2007), and the enabling role of thick sedimentary cover successions as part of a craton's lifecycle cannot be dismissed.

Importantly, thick continental mantle lithosphere acts as a long-term carbon sink (Sleep, 2009; Muirhead et al., 2020), as exemplified by the common presence of lithospheric diamond, especially beneath sub-Saharan Africa evident from the global database for diamond-bearing kimberlites and related rocks (Tappe et al., 2018). An integrated geophysical–geochemical model proposes 1–3 vol% diamond within the lowermost cratonic lithosphere (Garber et al., 2018), which would amount to a significant quantity of carbon that is unaccounted for in the most recent volatile budget for the lithospheric mantle (Gibson and McKenzie, 2023). Acknowledging craton roots as significant carbon repositories (Kelemen and Manning, 2015; Foley and Fischer, 2017), we suggest that a link between climatic perturbations and the emplacement of LIPs in cratonic regions is best established by additional $CO_2$ or $CH_4$ that can be released from ancient mantle lithospheres upon plume impingement, but $SO_2$ emissions from this geochemical reservoir play a relatively minor role.

## 5. Conclusions

- The newly identified 178.1 ± 8.4 Ma diamondiferous lamproite magmatic event in Zambia establishes a spatiotemporal link between low-volume ultrapotassic volcanism and the basalt-dominated Karoo LIP of sub-Saharan Africa. These so-called Kapamba lamproites erupted within the Permo–Triassic Luangwa Rift structure, but MgO-rich ultrapotassic magma formation was unrelated to rifting (ca. 270–230 Ma) and is best explained by plume–lithosphere interaction during the ca. 180 Ma LIP event.
- Strongly enriched olivine trace element and lamproite Sr–Nd–Hf–Pb isotope signatures suggest melt formation within a phlogopite-metasomatized peridotitic mantle domain near the base of the cratonic lithosphere, at approximately 180–200 km depth. The mantle-like $\delta^7$Li compositions and radiogenic isotope models suggest that the Kapamba lamproites originated from a MARID-style metasomatized source, created circa one billion years ago by melt ingress from the underlying asthenosphere, but without significant involvement of recycled sediment. Although lithospheric mantle source enrichment occurred in conjunction with collisional tectonics during which the cratonic assembly of sub-Saharan Africa formed, the absence of recycled sediment components in the Kapamba and other 'anorogenic' lamproites contrasts the origin of much shallower-sourced 'orogenic' lamproites.
- Plume-sourced flood basalt magmas of the Karoo LIP encountered MARID-style metasomatized peridotitic lithosphere en route to surface inheriting uniquely enriched incompatible element and radiogenic isotope signatures. Based on Nd–Hf isotope mass balance, up to 25% of MARID-sourced lamproite melt component contributed to some of the high-Ti flood volcanic units including alkali-rich picrites, which provides geochemical evidence for plume–lithosphere interactions. Although this mode of craton reactivation can remobilize significant amounts of volatiles, possible climatic effects caused by LIP-related carbon emissions from the continental mantle lithosphere are unlikely to be surpassed by those previously ascribed to $SO_2$ outgassing. In other words, the excess $SO_2$ required to explain the episode of global atmospheric cooling during the early Jurassic was probably sourced from LIP-impacted sedimentary successions at Earth's surface, with little or no influence by plume–lithosphere interaction at mantle depth.

## Declaration of Competing Interest

The authors declare that they have no known competing financial interests or personal relationships that could have appeared to influence the work reported in this paper.

## Acknowledgments

ST acknowledges financial support during 2018–2021 from the National Research Foundation of South Africa (NRF) and the Geological Society of South Africa (CIMERA and REI grants, respectively). NSN was supported through a PhD scholarship from the NRF. The ionprobe analytical work in Heidelberg (Germany) was financially assisted through NRF-ERTTG Grant No. 129811, awarded to ST. Henriette Ueckermann (University of Johannesburg), Allan Wilson (University of the Witwatersrand), Felix Genske (University of Münster) and Bettina Hübner (GFZ Potsdam) are thanked for technical support during our analytical program. This manuscript was initiated during the senior author's research sabbatical at the University of Münster in the autumn of 2021, which was financially supported by an Alexander von Humboldt Foundation alumni fellowship. Discussions with Joshua Davies, Katie Smart and Arto Luttinen over the course of this study are greatly appreciated. Troels Nielsen is thanked for providing the 'young' perovskite crystal from the Gardiner intrusion, used in this study as a SIMS U/Pb standard for data quality control. The helpful journal reviews by N. Arndt, L. Krmíček and two anonymous peers are kindly acknowledged. T. Magna and J. Catalano are thanked for efficient editorial handling.

## Appendix A. Supplementary Material

The Supplementary Material to this article comprises two files, in which the Analytical Methods are described *(Supplementary file A)* and the complete Dataset is reported *(Supplementary file B)*. The Analytical Methods also include results obtained for the measurements of standards and certified reference materials. The Dataset includes a tabulation of all analytical data generated during this study, such as U-Pb perovskite geochronology, bulk-rock geochemistry including Sr-Nd-Hf-Pb-Li isotopic compositions, olivine major and trace element compositions, and MARID xenoliths sulphur concentrations. The Dataset also lists the parameters used for isotope modelling. Supplementary Material to this article can be found online at https://doi.org/10.1016/j.gca.2023.04.008.

## References

Ammannati, E., Jacob, D.E., Avanzinelli, R., Foley, S.F., Conticelli, S., 2016. Low Ni olivine in silica-undersaturated ultrapotassic igneous rocks as evidence for carbonate metasomatism in the mantle. Earth Planet. Sci. Lett. 444, 64–74.

Angielczyk, K.D., Steyer, J.-S., Sidor, C.A., Smith, R.M.H., Whatley, R.L., Tolan, S., 2014. Permian and Triassic Dicynodont (Therapsida: Anomodontia) faunas of the Luangwa Basin, Zambia: Taxonomic update and implications for Dicynodont biogeography and biostratigraphy. In: Kammerer, C.F., Angielczyk, K.D., Fröbisch, J. (Eds.), Early evolutionary history of the Synapsida. Springer, Heidelberg, pp. 93–138.

Araoka, D., Kawahata, H., Takagi, T., Watanabe, Y., Nishimura, K., Nishio, Y., 2014. Lithium and strontium isotopic systematics in playas in Nevada, USA: Constraints on the origin of lithium. Miner. Depos. 49 (3), 371–379.

Arndt, N.T., Czamanske, G.K., Wooden, J.L., Fedorenko, V.A., 1993. Mantle and crustal contributions to continental flood volcanism. Tectonophysics 223 (1–2), 39–52.

Aulbach, S., Mungall, J.E., Pearson, D.G., 2016. Distribution and processing of highly siderophile elements in cratonic mantle lithosphere. In: Harvey, J., Day, J.M.D. (Eds.), Highly siderophile and strongly chalcophile elements in high-temperature geochemistry and cosmochemistry. Mineralogical Society of America, Chantilly, pp. 239–304.

Aulbach, S., Sun, J., Tappe, S., Höfer, H.E., Gerdes, A., 2017. Volatile-rich metasomatism in the cratonic mantle beneath SW Greenland: Link to kimberlites and mid-lithospheric discontinuities. J. Petrol. 58 (12), 2311–2338.

Banks, N.L., Bardwell, K.A., Musiwa, S., 1995. Karoo rift basins of the Luangwa Valley, Zambia. Geol. Soc. London Spec. Publ. 80, 285–295.

Batumike, J.M., Griffin, W.L., Belousova, E.A., Pearson, N.J., O'Reilly, S.Y., Shee, S.R., 2008. LAM-ICPMS U-Pb dating of kimberlitic perovskite: Eocene-Oligocene kimberlites from the Kundelungu Plateau, D.R. Congo. Earth Planet. Sci. Lett. 267 (3–4), 609–619.

Becker, M., le Roex, A.P., 2006. Geochemistry of South African on- and off-craton, Group I and Group II kimberlites: Petrogenesis and source region evolution. J. Petrol. 47 (4), 673–703.

Black, B.A., Karlstroim, L., Mather, T.A., 2021. The life cycle of large igneous provinces. Nat. Rev. Earth Env. 2 (12), 840–857.

Burke, K., Dewey, J.F., 1973. Triple junctions: Key indicators in applying plate tectonics to old rocks. J. Geol. 81 (4), 406–433.

Capriolo, M., Marzoli, A., Aradi, L.E., Callegaro, S., Dal Corso, J., Newton, R.J., Mills, B.J. W., Wignall, P.B., Bartoli, O., Baker, D.R., Youbi, N., Remusat, L., Spiess, R., Szabó, C., 2020. Deep CO2 in the end-Triassic Central Atlantic Magmatic Province. Nat. Commun. 11, 1670.

Carlson, R.W., Lugmair, G.W., Macdougall, J.D., 1981. Crustal influence in the generation of continental flood basalts. Nature 289 (5794), 160–162.

Catuneanu, O., Wopfner, H., Eriksson, P.G., Cairncross, B., Rubidge, B.S., Smith, R.M.H., Hancox, P.J., 2005. The Karoo basins of south-central Africa. J. Afr. Earth Sci. 43 (1–3), 211–253.

Celli, N.L., Lebedev, S., Schaeffer, A.J., Gaina, C., 2020. African cratonic lithosphere carved by mantle plumes. Nat. Commun. 11 (1), 1–10.

Chalapathi Rao, N.V., Lehmann, B., 2011. Kimberlites, flood basalts and mantle plumes: New insights from the Deccan large igneous province. Earth-Sci. Rev. 107 (3–4), 315–324.

Coffin, M.F., Eldholm, O., 1992. Volcanism and continental breakup: A global compilation of large igneous provinces. Geol. Soc. London Spec. Publ. 68, 17–30.

Cox, K.G., 1992. Karoo igneous activity, and the early stages of the breakup of Gondwanaland. Geol. Soc. London Spec. Publ. 68, 137–148.

Daly, M.C., Chorowicz, J., Fairhead, J.D., 1989. Rift basin evolution in Africa: The influence of reactivated steep basement shear zones. Geol. Soc. London Spec. Publ. 44, 309–334.

Davies, G.R., Stolz, A.J., Mahotkin, I.L., Nowell, G.M., Pearson, D.G., 2006. Trace element and Sr-Pb-Nd-Hf isotope evidence for ancient, fluid-dominated enrichment of the source of Aldan shield lamproites. J. Petrol. 47 (6), 1119–1146.

Day, J.M.D., Nutt, K.L.R., Mendenhall, B., Peters, B.J., 2021. Temporally variable crustal contributions to primitive mantle-derived Columbia River Basalt Group magmas. Chem. Geol. 572, 120197.

De Waele, B., Liegeois, J.P., Nemchin, A.A., Tembo, F., 2006. Isotopic and geochemical evidence of Proterozoic episodic crustal reworking within the Irumide Belt of south-central Africa, the southern metacratonic boundary of an Archaean Bangweulu Craton. Precambrian Res. 148 (3–4), 225–256.

Ellam, R.M., Cox, K.G., 1991. An interpretation of Karoo picrite basalts in terms of interaction between asthenospheric magmas and the mantle lithosphere. Earth Planet. Sci. Lett. 105 (1–3), 330–342.

Ellam, R.M., Carlson, R.W., Shirey, S.B., 1992. Evidence from Re-Os isotopes for plume-lithosphere mixing in Karoo flood basalt genesis. Nature 359 (6397), 718–721.

Ernst, R.E., 2014. Large Igneous Provinces. Cambridge University Press, Cambridge.

Ernst, R.E., Davies, D.R., Jowitt, S.M., Campbell, I.H., 2018. When do mantle plumes destroy diamonds? Earth Planet Sci. Lett. 502, 244–252.

Ernst, R.E., Mruma, A., Söderlund, U., Halls, H.C., 2015. Evidence for the extension of the 180 Ma Karoo LIP of southern Africa northward into Zambia and Tanzania. AGU Joint Assembly, Montreal (Canada), Abstract VGP34A-0414.

Fitzpayne, A., Giuliani, A., Hergt, J., Phillips, D., Janney, P.E., 2018. New geochemical constraints on the origins of MARID and PIC rocks: Implications for mantle metasomatism and mantle-derived potassic magmatism. Lithos 318, 478–493.

Fitzpayne, A., Giuliani, A., Harris, C., Thomassot, E., Cheng, C., Hergt, J., 2019a. Evidence for subduction-related signatures in the southern African lithosphere from the N-O isotopic composition of metasomatic mantle minerals. Geochim. Cosmochim. Acta 266, 237–257.

Fitzpayne, A., Giuliani, A., Maas, R., Hergt, J., Janney, P.E., Phillips, D., 2019b. Progressive metasomatism of the mantle by kimberlite melts: Sr-Nd-Hf-Pb isotope compositions of MARID and PIC minerals. Earth Planet. Sci. Lett. 509, 15–26.

Fitzpayne, A., Prytulak, J., Giuliani, A., Hergt, J., 2020. Thallium isotopic composition of phlogopite in kimberlite-hosted MARID and PIC mantle xenoliths. Chem. Geol. 531, 119347.

Foley, S.F., 1992. Vein-plus-wall-rock melting mechanism in the lithosphere and the origin of potassic alkaline magmas. Lithos 28, 435–453.

Foley, S.F., Fischer, T.P., 2017. An essential role for continental rifts and lithosphere in the deep carbon cycle. Nat. Geosci. 10, 897–902.

Foley, S.F., Wheller, G.E., 1990. Parallels in the origin of the geochemical signatures of island arc volcanics and continental potassic igneous rocks: The role of residual titanates. Chem. Geol. 85, 1–18.

Foley, S.F., Jacob, D.E., O'Neill, H.S.C., 2011. Trace element variations in olivine phenocrysts from Ugandan potassic rocks as clues to the chemical characteristics of parental magmas. Contrib. Mineral. Petrol. 162 (1), 1–20.

Foley, S.F., Prelevic, D., Rehfeldt, T., Jacob, D.E., 2013. Minor and trace elements in olivines as probes into early igneous and mantle melting processes. Earth Planet. Sci. Lett. 363, 181–191.

Fraser, K.J., Hawkesworth, C.J., Erlank, A.J., Mitchell, R.H., Scott Smith, B.H., 1985. Sr, Nd and Pb isotope and minor element geochemistry of lamproites and kimberlites. Earth Planet. Sci. Lett. 76 (1–2), 57–70.

Gallagher, K., Hawkesworth, C., 1992. Dehydration melting and the generation of continental flood basalts. Nature 358 (6381), 57–59.

Ganino, C., Arndt, N.T., 2009. Climate changes caused by degassing of sediments during the emplacement of large igneous provinces. Geology 37 (4), 323–326.

Garber, J.M., Maurya, S., Hernandez, J.A., Duncan, M.S., Zeng, L., Zhang, H.L., Faul, U., McCammon, C.A., Montagner, J.P., Moresi, L., Romanowicz, B.A., Rudnick, R.L.,

Stixrude, L., 2018. Multidisciplinary constraints on the abundance of diamond and eclogite in the cratonic lithosphere. Geochem. Geophys. Geosyst. 19, 2062–2086.
Gibson, S.A., McKenzie, D., 2023. On the role of Earth's lithospheric mantle in global volatile cycles. Earth Planet. Sci. Lett. 602, 117946.
Gibson, S.A., Thompson, R.N., Dickin, A.P., Leonardos, O.H., 1996. High-Ti and low-Ti mafic potassic magmas: Key to plume-lithosphere interactions and continental flood-basalt genesis. Earth Planet. Sci. Lett. 141 (1–4), 325–341.
Giuliani, A., Phillips, D., Maas, R., Woodhead, J.D., Kendrick, M.A., Greig, A., Armstrong, R.A., Chew, D., Kamenetsky, V.S., Fiorentini, M.L., 2014. LIMA U-Pb ages link lithospheric mantle metasomatism to Karoo magmatism beneath the Kimberley region, South Africa. Earth Planet. Sci. Lett. 401, 132–147.
Giuliani, A., Phillips, D., Woodhead, J.D., Kamenetsky, V.S., Fiorentini, M.L., Maas, R., Soltys, A., Armstrong, R.A., 2015. Did diamond-bearing orangeites originate from MARID-veined peridotites in the lithospheric mantle? Nat. Commun. 6, 1–10.
Goscombe, B., Foster, D.A., Gray, D., Wade, B., 2020. Assembly of central Gondwana along the Zambezi Belt: Metamorphic response and basement reactivation during the Kuunga Orogeny. Gondwana Res. 80, 410–465.
Greber, N.D., Davies, J.H.F.L., Gaynor, S.P., Jourdan, F., Bertrand, H., Schaltegger, U., 2020. New high precision U-Pb ages and Hf isotope data from the Karoo large igneous province: Implications for pulsed magmatism and early Toarcian environmental perturbations. Results Geochem. 1, 100005.
Grégoire, M., Bell, D.R., le Roex, A.P., 2002. Trace element geochemistry of phlogopite-rich mafic mantle xenoliths: Their classification and their relationship to phlogopite-bearing peridotites and kimberlites revisited. Contrib. Mineral. Petrol. 142 (5), 603–625.
Griffin, W.L., Batumike, J.M., Greau, Y., Pearson, N.J., Shee, S.R., O'Reilly, S.Y., 2014. Emplacement ages and sources of kimberlites and related rocks in southern Africa: U-Pb ages and Sr-Nd isotopes of groundmass perovskite. Contrib. Mineral. Petrol. 168 (1), 1–13.
Guex, J., Pilet, S., Muntener, O., Bartolini, A., Spangenberg, J., Schoene, B., Sell, B., Schaltegger, U., 2016. Thermal erosion of cratonic lithosphere as a potential trigger for mass-extinction. Sci. Rep. 6, 9.
Halama, R., McDonough, W.F., Rudnick, R.L., Bell, K., 2008. Tracking the lithium isotopic evolution of the mantle using carbonatites. Earth Planet. Sci. Lett. 265 (3–4), 726–742.
Halls, H.C., Burns, K.G., Bullock, S.J., Batterham, P.M., 1987. Mafic dyke swarms of Tanzania interpreted from aeromagnetic data. In: Halls, H.C., Fahrig, W.F. (Eds.), Mafic dyke swarms. Geological Association of Canada Special Paper, pp. 173–186.
Harmer, R.E., Nex, P.A.M., 2016. Rare Earth deposits of Africa. Episodes 39 (2), 381–406.
Harmer, R.E., Lee, C.A., Eglington, B.M., 1998. A deep mantle source for carbonatite magmatism: Evidence from the nephelinites and carbonatites of the Buhera District, SE Zimbabwe. Earth Planet. Sci. Lett. 158 (3–4), 131–142.
Harris, C., le Roux, P., Cochrane, R., Martin, L., Duncan, A.R., Marsh, J.S., le Roex, A.P., Class, C., 2015. The oxygen isotope composition of Karoo and Etendeka picrites: High delta O-18 mantle or crustal contamination? Contrib. Mineral. Petrol. 170 (1), 24.
Heimdal, T.H., Jones, M.T., Svensen, H.H., 2020. Thermogenic carbon release from the Central Atlantic Magmatic Province caused major end-Triassic carbon cycle perturbations. Proc. Natl. Acad. Sci. U. S. A. 117 (22), 11968–11980.
Heinonen, J.S., Fusswinkel, T., 2017. High Ni and low Mn/Fe in olivine phenocrysts of the Karoo meimechites do not reflect pyroxenitic mantle sources. Chem. Geol. 467, 134–142.
Heinonen, J.S., Carlson, R.W., Luttinen, A.V., 2010. Isotopic (Sr, Nd, Pb, and Os) composition of highly magnesian dikes of Vestfjella, western Dronning Maud Land, Antarctica: A key to the origins of the Jurassic Karoo large igneous province? Chem. Geol. 277 (3–4), 227–244.
Heinonen, J.S., Luttinen, A.V., Bohrson, W.A., 2016. Enriched continental flood basalts from depleted mantle melts: Modeling the lithospheric contamination of Karoo lavas from Antarctica. Contrib. Mineral. Petrol. 171 (1).
Hoare, B.C., O'Sullivan, G., Tomlinson, E.L., 2021. Metasomatism of the Kaapvaal Craton during Cretaceous intraplate magmatism revealed by combined zircon U-Pb isotope and trace element analysis. Chem. Geol. 578, 120302.
Hofmann, C., Courtillot, V., Feraud, G., Rochette, P., Yirgu, G., Ketefo, E., Pik, R., 1997. Timing of the Ethiopian flood basalt event and implications for plume birth and global change. Nature 389 (6653), 838–841.
Hopp, J., Trieloff, M., Brey, G.P., Woodland, A.B., Simon, N.S.C., Wijbrans, J.R., Siebel, W., Reitter, E., 2008. Ar-40/Ar-39-ages of phlogopite in mantle xenoliths from South African kimberlites: Evidence for metasomatic mantle impregnation during the Kibaran orogenic cycle. Lithos 106 (3–4), 351–364.
Howarth, G.H., Giuliani, A., 2020. Contrasting types of micaceous kimberlite-lamproite magmatism from the Man Craton (West Africa): New insights from petrography and mineral chemistry. Lithos 362, 105483.
Howarth, G.H., Giuliani, A., Soltys, A., Bussweiler, Y., 2022. Compositional variations in primitive kimberlite melts and entrained mantle cargo from a global survey of trace element compositions in kimberlite olivine. J. Petrol. 63 (8) egac062.
Howarth, G.H., Harris, C., 2017. Discriminating between pyroxenite and peridotite sources for continental flood basalts (CFB) in southern Africa using olivine chemistry. Earth Planet. Sci. Lett. 475, 143–151.
Huang, Y.M., Van Calsteren, P., Hawkesworth, C.J., 1995. The evolution of the lithosphere in southern Africa: A perspective on the basic granulite xenoliths from kimberlites in South Africa. Geochim. Cosmochim. Acta 59 (23), 4905–4920.
Jaques, A.L., Foley, S.F., 2018. Insights into the petrogenesis of the West Kimberley lamproites from trace elements in olivine. Mineral. Petrol. 112, 519–537.
Jourdan, F., Bertrand, H., Scharer, U., Blichert-Toft, J., Feraud, G., Kampunzu, A.B., 2007. Major and trace element and Sr, Nd, Hf and Pb isotope compositions of the Karoo large igneous province, Botswana-Zimbabwe: Lithosphere vs mantle plume contribution. J. Petrol. 48 (6), 1043–1077.
Kasbohm, J., Schoene, B., 2018. Rapid eruption of the Columbia River flood basalt and correlation with the mid-Miocene climate optimum. Sci. Adv. 4 (9) eaat8223.
Kelemen, P.B., Manning, C.E., 2015. Reevaluating carbon fluxes in subduction zones, what goes down, mostly comes up. Proc. Natl. Acad. Sci. U. S. A. 112 (30), 3997–4006.
Kinny, P.D., Griffin, B.J., Heaman, L.M., Brakhfogel, F.F., Spetsius, Z.V., 1997. SHRIMP U-Pb ages of perovskite from Yakutian kimberlites. In: Sobolev, N.V., Mitchell, R.H. (Eds.), Proceedings of the Sixth International Kimberlite Conference. Allerton Press, New York, United States, pp. 97–105.
Konzett, J., Sweeney, R.J., Thompson, A.B., Ulmer, P., 1997. Potassium amphibole stability in the upper mantle: An experimental study in a peralkaline KNCMASH system to 8.5 GPa. J. Petrol. 38 (5), 537–568.
Krienitz, M.S., Garbe-Schönberg, C.D., Romer, R.L., Meixner, A., Haase, K.M., Stroncik, N.A., 2012. Lithium isotope variations in ocean island basalts: Implications for the development of mantle heterogeneity. J. Petrol. 53 (11), 2333–2347.
Krmíček, L., Romer, R.L., Ulrych, J., Glodny, J., Prelevic, D., 2016. Petrogenesis of orogenic lamproites of the Bohemian Massif: Sr–Nd–Pb–Li isotope constraints for Variscan enrichment of ultra-depleted mantle domains. Gondwana Res. 35, 198–216.
Krmíček, L., Romer, R.L., Timmerman, M.J., Ulrych, J., Glodny, J., Prichystal, A., Sudo, M., 2020. Long-lasting (65 Ma) regionally contrasting late- to post-orogenic Variscan mantle-derived potassic magmatism in the Bohemian Massif. J. Petrol. 61 (7) egaa072.
Krmíček, L., Magna, T., Pandey, A., Chalapathi Rao, N.V., Kynicky, J., 2022. Lithium isotopes in kimberlites, lamproites and lamprophyres as tracers of source components and processes related to supercontinent cycles. Geol. Soc. London, Spec. Publ. 513 (1), 209–236.
Larsen, L.M., Pedersen, A.K., Sundvoll, B., Frei, R., 2003. Alkali picrites formed by melting of old metasomatized lithospheric mantle: Manitdlat Member, Vaigat Formation, Palaeocene of West Greenland. J. Petrol. 44 (1), 3–38.
Liu, J.Q., Chen, L.H., Wang, X.J., Zhang, X.Y., Zeng, G., Erdmann, S., Murphy, D.T., Collerson, K.D., Komiya, T., Krmíček, L., 2022. Magnesium and zinc isotopic evidence for the involvement of recycled carbonates in the petrogenesis of Gaussberg lamproites, Antarctica. Chem. Geol. 609, 121067.
Lustrino, M., Fedele, L., Agostini, S., Prelevic, D., Salari, G., 2019. Leucitites within and around the Mediterranean area. Lithos 324, 216–233.
Luttinen, A.V., 2018. Bilateral geochemical asymmetry in the Karoo large igneous province. Sci. Rep. 8, 1–11.
Luttinen, A.V., Zhang, X., Foland, K.A., 2002. 159 Ma Kjakebeinet lamproites (Dronning Maud Land, Antarctica) and their implications for Gondwana breakup processes. Geol. Mag. 139 (5), 525–539.
McKenzie, D., 1989. Some remarks on the movement of small melt fractions in the mantle. Earth Planet. Sci. Lett. 95 (1–2), 53–72.
Mirnejad, H., Bell, K., 2006. Origin and source evolution of the Leucite Hills lamproites: Evidence from Sr-Nd-Pb-O isotopic compositions. J. Petrol. 47 (12), 2463–2489.
Muirhead, J.D., Fischer, T.P., Oliva, S.J., Laizer, A., van Wijk, J., Currie, C.A., Lee, H., Judd, E.J., Kazimoto, E., Sano, Y., Takahata, N., Tiberi, C., Foley, S.F., Dufek, J., Reiss, M.C., Ebinger, C.J., 2020. Displaced cratonic mantle concentrates deep carbon during continental rifting. Nature 582 (7810), 67–72.
Müller, R.D., Cannon, J., Qin, X.D., Watson, R.J., Gurnis, M., Williams, S., Pfaffelmoser, T., Seton, M., Russell, S.H.J., Zahirovic, S., 2018. GPlates: Building a virtual Earth through deep time. Geochem. Geophys. Geosyst. 19 (7), 2243–2261.
Murphy, D.T., Collerson, K.D., Kamber, B.S., 2002. Lamproites from Gaussberg, Antarctica: Possible transition zone melts of Archaean subducted sediments. J. Petrol. 43 (6), 981–1001.
Nelson, D.R., McCulloch, M.T., Sun, S.S., 1986. The origins of ultrapotassic rocks as inferred from Sr, Nd and Pb isotopes. Geochim. Cosmochim. Acta 50 (2), 231–245.
Ngwenya, N.S., Tappe, S., 2021. Diamondiferous lamproites of the Luangwa Rift in central Africa and links to remobilized cratonic lithosphere. Chem. Geol. 568, 120019.
O'Brien, H.E., Irving, A.J., McCallum, I.S., Thirlwall, M.F., 1995. Strontium, neodymium, and lead isotope evidence for the interaction of post-subduction asthenospheric potassic mafic magmas of the Highwood Mountains, Montana, USA, with ancient Wyoming craton lithospheric mantle. Geochim. Cosmochim. Acta 59 (21), 4539–4556.
O'Donnell, J.P., Selway, K., Nyblade, A.A., Brazier, R.A., El Tahir, N., Durrheim, R.J., 2016. Thick lithosphere, deep crustal earthquakes and no melt: A triple challenge to understanding extension in the western branch of the East African Rift. Geophys. J. Int. 204 (2), 985–998.
Palme, H., O'Neill, H.S.C., 2003. Cosmochemical estimates of mantle composition. In: Carlson, R.W. (Ed.), Treatise on Geochemistry. Elsevier, Amsterdam, pp. 1–38.
Pintér, Z., Foley, S.F., Yaxley, G.M., 2022. Diamonds, dunites, and metasomatic rocks formed by melt/rock reaction in craton roots. Commun. Earth Environ. 3 (296), 1–8.
Plank, T., 2014. The chemical composition of subducting sediments. Treatise Geochem. 4, 607–629.
Prelevic, D., Stracke, A., Foley, S.F., Romer, R.L., Conticelli, S., 2010. Hf isotope compositions of Mediterranean lamproites: Mixing of melts from asthenosphere and crustally contaminated mantle lithosphere. Lithos 119 (3–4), 297–312.
Prelevic, D., Foley, S.F., Jacob, D.E., 2013. Recycling plus: A new recipe for the formation of Alpine-Himalayan orogenic mantle lithosphere. Earth Planet. Sci. Lett. 362, 187–197.
Rasmussen, M.B., Halldorsson, S.A., Gibson, S.A., Gudfinnsson, G.H., 2020. Olivine chemistry reveals compositional source heterogeneities within a tilted mantle plume beneath Iceland. Earth Planet. Sci. Lett. 531, 116008.

Riley, T.R., Leat, P.T., Curtis, M.L., Millar, I.L., Duncan, R.A., Fazel, A., 2005. Early-Middle Jurassic dolerite dykes from western Dronning Maud Land (Antarctica): Identifying mantle sources in the Karoo large igneous province. J. Petrol. 46 (7), 1489–1524.

Rooney, T.O., 2020. The Cenozoic magmatism of East Africa: Part III – Rifting of the craton. Lithos 360–361, 105390.

Rosenthal, A., Foley, S.F., Pearson, D.G., Nowell, G.M., Tappe, S., 2009. Petrogenesis of strongly alkaline primitive volcanic rocks at the propagating tip of the western branch of the East African Rift. Earth Planet. Sci. Lett. 284 (1–2), 236–248.

Sarafian, E., Evans, R.L., Abdelsalam, M.G., Atekwana, E., Elsenbeck, J., Jones, A.G., Chikambwe, E., 2018. Imaging Precambrian lithospheric structure in Zambia using electromagnetic methods. Gondwana Res. 54, 38–49.

Sarkar, S., Giuliani, A., Phillips, D., Howarth, G.H., Ghosh, S., Dalton, H., 2022. Sublithospheric melt input in cratonic lamproites. Geology 50 (11), 1296–1300.

Scott Smith, B.H., Skinner, E.M.W., Loney, P.E., 1989. The Kapamba lamproites of the Luangwa Valley, eastern Zambia. In: Ross, J. (Ed.) Kimberlites and Related Rocks. Blackwell (Geological Society of Australia Special Publication No.14/1), Victoria, pp. 189–205.

Sleep, N.H., 2009. Stagnant lid convection and carbonate metasomatism of the deep continental lithosphere. Geochem. Geophys. Geosyst. 10, Q11010.

Smart, K.A., Tappe, S., Ishikawa, A., Pfänder, J.A., Stracke, A., 2019. K-rich hydrous mantle lithosphere beneath the Ontong Java Plateau: Significance for the genesis of oceanic basalts and Archean continents. Geochim. Cosmochim. Acta 248, 311–342.

Smith, C.B., Clark, T.C., Barton, E.S., Bristow, J.W., 1994. Emplacement ages of kimberlite occurrences in the Prieska region, southwest border of the Kaapvaal Craton, South Africa. Chem. Geol. 113 (1–2), 149–169.

Sobolev, A.V., Hofmann, A.W., Kuzmin, D.V., Yaxley, G.M., Arndt, N.T., Chung, S.L., Danyushevsky, L.V., Elliott, T., Frey, F.A., Garcia, M.O., Gurenko, A.A., Kamenetsky, V.S., Kerr, A.C., Krivolutskaya, N.A., Matvienkov, V.V., Nikogosian, I. K., Rocholl, A., Sigurdsson, I.A., Sushchevskaya, N.M., Teklay, M., 2007. The amount of recycled crust in sources of mantle-derived melts. Science 316 (5823), 412–417.

Sobolev, S.V., Sobolev, A.V., Kuzmin, D.V., Krivolutskaya, N.A., Petrunin, A.G., Arndt, N. T., Radko, V.A., Vasiliev, Y.R., 2011. Linking mantle plumes, large igneous provinces and environmental catastrophes. Nature 477 (7364), 312–316.

Stracke, A., 2012. Earth's heterogeneous mantle: A product of convection-driven interaction between crust and mantle. Chem. Geol. 330–331, 274–299.

Sun, J., Liu, C.-Z., Tappe, S., Kostrovitsky, S.I., Wu, F.-Y., Yakovlev, D., Yang, Y.H., Yang, J.H., 2014. Repeated kimberlite magmatism beneath Yakutia and its relationship to Siberian flood volcanism: Insights from in situ U-Pb and Sr-Nd perovskite isotope analysis. Earth Planet. Sci. Lett. 404, 283–295.

Svensen, H., Planke, S., Chevallier, L., Malthe-Sørenssen, A., Corfu, F., Jamtveit, B., 2007. Hydrothermal venting of greenhouse gases triggering Early Jurassic global warming. Earth Planet. Sci. Lett. 256 (3–4), 554–566.

Tappe, S., Foley, S.F., Stracke, A., Romer, R.L., Kjarsgaard, B.A., Heaman, L.M., Joyce, N., 2007. Craton reactivation on the Labrador Sea margins: $^{40}Ar/^{39}Ar$ age and Sr–Nd–Hf–Pb isotope constraints from alkaline and carbonatite intrusives. Earth Planet. Sci. Lett. 256, 433–454.

Tappe, S., Foley, S.F., Kjarsgaard, B.A., Romer, R.L., Heaman, L.M., Stracke, A., Jenner, G.A., 2008. Between carbonatite and lamproite: Diamondiferous Torngat ultramafic lamprophyres formed by carbonate-fluxed melting of cratonic MARID-type metasomes. Geochim. Cosmochim. Acta 72 (13), 3258–3286.

Tappe, S., Romer, R.L., Stracke, A., Steenfelt, A., Smart, K.A., Muehlenbachs, K., Torsvik, T.H., 2017. Sources and mobility of carbonate melts beneath cratons, with implications for deep carbon cycling, metasomatism and rift initiation. Earth Planet. Sci. Lett. 466, 152–167.

Tappe, S., Smart, K.A., Torsvik, T.H., Massuyeau, M., de Wit, M.C.J., 2018. Geodynamics of kimberlites on a cooling Earth: Clues to plate tectonic evolution and deep volatile cycles. Earth Planet. Sci. Lett. 484, 1–14.

Tappe, S., Budde, G., Stracke, A., Wilson, A., Kleine, T., 2020. The tungsten-182 record of kimberlites above the African superplume: Exploring links to the core-mantle boundary. Earth Planet. Sci. Lett. 547, 116473.

Tappe, S., Shaikh, A.M., Wilson, A.H., Stracke, A., 2022. Evolution of ultrapotassic volcanism on the Kaapvaal craton: deepening the orangeite versus lamproite debate. Geol. Soc. London Spec. Publ. 513, 17–44.

Thompson, R.N., Gibson, S.A., 1991. Subcontinental mantle plumes, hotspots and pre-existing thinspots. J. Geol. Soc. (London, U.K.) 148, 973–977.

Tian, S.H., Hou, Z.Q., Mo, X.X., Tian, Y.H., Zhao, Y., Hou, K.J., Yang, Z.S., Hu, W.J., Li, X. F., Zhang, Y.J., 2020. Lithium isotopic evidence for subduction of the Indian lower crust beneath southern Tibet. Gondwana Res. 77, 168–183.

Tomascak, P.B., Magna, T., Dohmen, R., 2016. Advances in lithium isotope geochemistry. Springer, Heidelberg.

Turunen, S.T., Luttinen, A.V., Heinonen, J.S., Jamal, D.L., 2019. Luenha picrites, Central Mozambique: Messengers from a mantle plume source of Karoo continental flood basalts? Lithos 346, 105152.

Veter, M., Foley, S.F., Mertz-Kraus, R., Groschopf, N., 2017. Trace elements in olivine of ultramafic lamprophyres controlled by phlogopite-rich mineral assemblages in the mantle source. Lithos 292, 81–95.

Wang, T., Feng, J.K., Liu, K.H., Gao, S.S., 2019. Crustal structure beneath the Malawi and Luangwa Rift Zones and adjacent areas from ambient noise tomography. Gondwana Res. 67, 187–198.

Wedmore, L.N.J., Biggs, J., Floyd, M., Fagereng, A., Mdala, H., Chindandali, P., Williams, J.N., Mphepo, F., 2021. Geodetic constraints on cratonic microplates and broad strain during rifting of thick southern African lithosphere. Geophys. Res. Lett. 48 (17) e2021GL093785.

White, R., McKenzie, D., 1989. Magmatism at rift zones: The generation of volcanic continental margins and flood basalts. J. Geophys. Res. 94 (B6), 7685–7729.